THE UNIVERSITY OF CHICAGO

THE VARIATIONAL TWO-ELECTRON REDUCED-DENSITY-MATRIX METHOD FOR EXTENDED SYSTEMS

A DISSERTATION SUBMITTED TO
THE FACULTY OF THE DIVISION OF THE PHYSICAL SCIENCES
IN CANDIDACY FOR THE DEGREE OF
DOCTOR OF PHILOSOPHY

DEPARTMENT OF CHEMISTRY

BY
NICHOLAS C. RUBIN

CHICAGO, ILLINOIS
MARCH 2016

To my sister Emily

TABLE OF CONTENTS

LIST OF FIGURES

LIST OF TABLES

ACKNOWLEDGMENTS

Completing this thesis would not have been possible without support from my colleagues, mentors, friends, and family. My undergraduate advisor once told me that the most successful graduate students are the ones with a strong support network. Given the clarity of hindsight, I full heartedly believe this to be true. I would like to acknowledge the role my support network has played and thank them for getting me to this point.

My dissertation would not have been possible without my advisor Professor David Mazziotti. His advising style, which gave me a great deal of independence, has allowed me to not only discover little bit about electronic structure by myself but given me the confidence and ability to independently solve any problem thrown my way.

The Mazziotti group, past and present, has been incredibly enjoyable to work with over the years. A special thanks to Jay Foley and Srikant Veeraraghaven for being understanding and patient when I turned to them for help with theory and programming. Thank you to my group mates, Chad, Andrew, Erik, Anthony, Romit, Valentine, Erica, Ali, Manas, Kade, Alison, Charles, and Lexie. You all have made our work environment fun and lighthearted. It has been a pleasure working and learning with each and every one of you.

During my time at University of Illinois I was fortunate enough to have Professor Boulatov as my undergraduate advisor. Working in his research group for four years was one of the most educational and enjoyable parts of my time at UIUC. Beyond chemical concepts, he pressed me to evaluate my motivations for studying science and taught me critical investigation skills that I find useful to this day. For this I am eternally grateful.

Finally, I'd like to thank those closest to me. To my parents, thank you for your tireless support and guidance. All my successes can be attributed to the values you have instilled in me. To my friends, thank you for all the support you have given me and distractions you provided. And lastly, to Yihan, Toro, and Nimbus, through this process you have been more patient and understanding than I ever thought possible. Thank you for enhancing my life.

ABSTRACT

In this thesis we develop the variational two-electron reduced-density-matrix method for extended systems. Extended systems are represented in two ways: i) lattice models describing the dominant valence electronic structure with periodic boundaries to account for their extended nature and ii) a crystalline-orbital basis built from atomic orbitals using the generalization of molecular orbital theory to polymers.

The first part of this thesis (Ch. 3-4) examines the performance of the variational 2-RDM method on lattice systems with tunable electron correlation. The first of these systems is the classic Hubbard model with linear and ladder lattice topologies. Because electron correlation functions, such as charge- and spin-ordering, are linear functions of the 2-RDM, the difference in electronic structure between one- and quasi-one-dimensional systems is accurately characterized. The second model contains only two-body interactions and is unique among typical spin models in that it does not have a mean-field reference wave function. The ground state wave functions from all Hamiltonians in the model have the same 1-electron reduced density matrix; consequently, one-electron theories are largely inapplicable. The superconducting η-pairing ground states make the model a unique tool for demonstrating the necessary N-representability in highly correlated environments.

The second part of this thesis (Ch. 5-6) develops a formalism for modeling materials by solving the full Schrödinger equation. Crystalline-orbital Hartree-Fock provides a set of orbitals and integral tensors for the variational 2-RDM method. We demonstrate that time-reversal symmetry, which is implicitly included in position space electronic structure calculations, must be explicitly included as an N-representability constraint on the 2-RDM when using a momentum space basis. The necessity of these equality constraints is demonstrated by the accurate recovery of the binding energy of two polymers and the symmetry of their natural orbital occupations.

CHAPTER 1

INTRODUCTION

1.1 Simulating Electronic Structure

Theoretical chemistry is the attempt to construct mathematical methodologies to understand, simulate, and predict properties of molecules and materials. Electronic structure theory is a sub-field particularly related to the description of electrons and their dynamics. A complete *ab initio* description of a molecule's or material's electronic structure can be determined by solving the full non-relativistic time-independent Schrödinger equation (TISE)

$$\hat{H}\Psi(r) = E\Psi(r) \tag{1.1}$$

where $\hat{H}$ and $\Psi(r)$ are the N-electron Hamiltonian and wave function.

$$\hat{H} = -\sum_{i=1}^{N} \frac{1}{2}\nabla_i^2 - \sum_{A}\sum_{i=1}^{N} \frac{Z_A}{r_{iA}} + \sum_{i<j}^{N} \frac{1}{r_{ij}} \tag{1.2}$$

$$\hat{H} = \sum_{i=1}^{N} \hat{h}(i) + \sum_{i=1, j<i}^{N} \hat{V}(i,j) \tag{1.3}$$

The Hamiltonian contains the interaction operators for electrons in the static field of the nuclei. The operators are traditionally partitioned into two types: i) $h(i)$ which contains the kinetic energy and nuclear attraction one-electron operators and ii) $V(i,j)$ which contains the Coulomb interaction between two electrons. The electronic energy of an N-body quantum system (E) is the expectation value of the Hamiltonian in Eq. (1.1) with the N-body electron distribution. In general, exact solutions to the Schrödinger equation are prohibitively expensive to compute. As such, the role of a theoretical and computational chemist is to create methodologies that balance accuracy and computational expense for describing the

electronic structure of a system.

One approach is to throw away or down-fold all but the essential interactions terms of the Hamiltonian and perform accurate simulations on the resulting reduced system to gain insight into the valence electronic structure. In quantum chemistry and solid-state physics, this is a well justified approximation because properties such as bonding or conduction are described by valence electron behavior [22]. This down-folding method is essential for materials or polymers where the unit cell can have hundreds of electrons and the crystal is formally infinitely sized. Generating a minimal Hamiltonian that sufficiently describes the dominant features of the electronic structure in a molecule was the driving force behind the construction of the Hückel-model for conjugated hydrocarbons with π-orbital networks and its extension, which include electron correlation effects, the Pariser-Parr-Pople model [18, 19, 22]. These models have provided insight into valence properties of polymers such as bonding and their conductivity even when the exact description of the polymer unit cell is computationally out of reach. The Hubbard Hamiltonian is the physicist's paradigmatic example of a model system used to understand strongly correlated materials. Initially developed to describe the behavior of the t_{2g} bands in transition metal oxide crystals (FeO, NiO, CoO) [14], it has recently re-emerged as a possible model Hamiltonian for much more complicated electron behavior driven by strong correlation such as high-temperature superconductivity [1] and spin-liquids [5].

The thread connecting solving the electronic structure of model systems and the full unadulterated Schrödinger equation is the difficulty in treating two-body interactions and enforcing Fermi statistics on the electrons. The presence of the two-body interaction results in an N-electron distribution that cannot be decomposed into non-interacting one-electron parts. Determining methodologies that can accurately account for the non-separability of particle distributions is the central problem in quantum chemistry and solid-state physics.

1.2 Mean-field Solution

For a molecular system, solving the Schrödinger equation commonly starts with a procedure that posits the structure of the wave function as an antisymmetric product of one-electron orbitals and relaxes the two-body piece of the Hamiltonian. This procedure is known as the Hartree-Fock method [24]. The Hartree-Fock wave function is a Slater determinant of molecular orbitals, which are themselves linear combinations of atomic orbitals.

$$|\psi_0\rangle = \frac{1}{\sqrt{N!}} \begin{vmatrix} \phi_1(1) & \phi_2(1) & ... & \phi_N(1) \\ \phi_1(2) & \phi_2(2) & ... & \phi_N(2) \\ \vdots & & \ddots & \vdots \\ \phi_1(N) & \phi_2(N) & ... & \phi_N(N) \end{vmatrix} \tag{1.4}$$

$$\phi_i = \sum_{\mu} c_{i,\mu} \chi_{\mu} \tag{1.5}$$

In each iteration of the Hartree-Fock self-consistent-field (SCF) procedure, the lowest N-orbitals are used to construct a new average potential, which is then used to minimize a new set of atomic orbital coefficients. Upon convergence of the SCF procedure a set of orthogonal molecular orbitals that minimizes the Hartree-Fock energy are obtained. For lattice models, the mean-field procedure involves averaging the two-body operators, generating a summation of one-body operators. For example, the Hubbard interaction term can be decomposed by considering fluctuations around a mean value.

$$\Delta n_{i\sigma} = \hat{n}_{i,\sigma} - \langle \hat{n}_{i,\sigma} \rangle \tag{1.6}$$

$$\hat{n}_{i,\sigma} = \Delta n_{i\sigma} + \langle \hat{n}_{i,\sigma} \rangle \tag{1.7}$$

$$\hat{a}^\dagger_{i\alpha}\hat{a}_{i\alpha}\hat{a}^\dagger_{i\beta}\hat{a}_{i\beta} = [\Delta n_{i\alpha} + \langle \hat{n}_{i\alpha}\rangle]\left[\Delta n_{i\beta} + \langle \hat{n}_{i\beta}\rangle\right] \tag{1.8}$$

$$= \Delta n_{i\alpha}\Delta n_{i\beta} + \Delta n_{i\alpha}\langle \hat{n}_{i\beta}\rangle + \tag{1.9}$$

$$\langle \hat{n}_{i\alpha}\rangle \Delta n_{i\beta} + \langle \hat{n}_{i\alpha}\rangle\langle \hat{n}_{i\beta}\rangle \tag{1.10}$$

$$= \langle n_{i\beta}\rangle \left(\Delta n_{i\alpha} + \langle n_{i\alpha}\rangle - \frac{1}{2}\langle n_{i\alpha}\rangle\right) \tag{1.11}$$

$$+\langle n_{i\alpha}\rangle \left(\Delta n_{i\beta} + \langle n_{i\beta}\rangle - \frac{1}{2}\langle n_{i\beta}\rangle\right) \tag{1.12}$$

$$= \hat{n}_{i\alpha}\langle \hat{n}_{i\beta}\rangle + \hat{n}_{i\beta}\langle \hat{n}_{i\alpha}\rangle - \langle \hat{n}_{i\alpha}\rangle\langle \hat{n}_{i\beta}\rangle \tag{1.13}$$

$$U\hat{n}_\alpha\hat{n}_\beta \approx U\left(\hat{n}_\alpha\langle n_\beta\rangle + \hat{n}_\beta\langle n_\alpha\rangle - \langle n_\alpha\rangle\langle n_\beta\rangle\right) \tag{1.14}$$

Making the above substitution in the Hubbard Hamiltonian results in a one-body operator. Simple diagonalization leads to a set of 1-electron orbitals.

1.3 Exact Solution

An exact solution to the Schrödinger equation (Eq. 1.1) can be determined by minimizing the energy of the Hamiltonian with respect to the N-body wave function expanded in a one-particle basis. Although this sounds simple as stated, enumerating the full N-body wave function has factorial scaling with system size. We define the N-body wave function as

$$|\psi_{\text{FCI}}\rangle = |\psi_0\rangle + \sum_{ab} c_a^b \hat{a}_b^\dagger \hat{a}_a |\psi_0\rangle + \sum_{a<b;r<s} c_{ab}^{rs} \hat{a}_r^\dagger \hat{a}_s^\dagger \hat{a}_b \hat{a}_a |\psi_0\rangle + ... \tag{1.15}$$

where $|\psi_0\rangle$ is the Hartree-Fock wave function and $\hat{a}_i^\dagger$ ($\hat{a}_i$) is the creation (annihilation) operator from second quantization for the single particle state i, which produces a different determinant within the single-particle orbital space. The coefficients $\{c_a^b, c_{ab}^{rs}, ...\}$ correspond to the amplitude that each determinant contributes to the correlated N-electron wave func-

tion. For an N-electron system with r spatial orbitals, the number of determinants scales as a factorial of the basis size (r) [24, 11].

$$\#\text{ of Dets} = \binom{2r}{N} = \frac{2r!}{N!(2r-N)!} \tag{1.16}$$

The number of determinants grows extremely rapidly restricting an exact solution to the smallest of systems. Even if the Hamiltonian in a determinant basis can be fit into computer memory with clever sparsity or compression, solving the generalized eigenvalue equation corresponding to the energy minimization scales cubically with the linear dimension of the matrix. Though there are clever iterative techniques that project out the m lowest eigenvalues such as the power method [10], Lanczos [16], Arnoldi [20], and Davidson [6] the factorial scaling quickly renders even these solvers inapplicable.

One may ask why it is necessary to go through the trouble of parametrizing a solution space that has factorial scaling. Excluding electron correlation effects captured by the FCI expansion results in electronic structure that is qualitatively incorrect. For example, electron correlation causes metal-oxides to be insulators when predicted to be metals from band-theory (a single particle theory) [14]. The mean-field approximation is especially inadequate for the lattice models investigated in Chapters 3 and 4. When the averaging procedure is applied to models with local two-body interactions, such as the Hubbard model, the resulting one-electron operator Hamiltonian has a free-particle ground state with band energies shifted by the interaction parameter U. The free particle band picture is completely at odds with the localized electron large U limit of the Hubbard model [17]. The amount of lost information can be quantified by defining the energy difference between the exact solution and the reference mean-field solution as correlation energy.

$$E_{\text{corr}} = E_{\text{FCI}} - E_{\text{HF}} \tag{1.17}$$

Correlation energy can be classified into two types. The first type, *dynamic correlation*, corresponds to the mutual instantaneous repulsion between two electrons. The second type, *static correlation*, stems from the fact that multiple determinants are necessary to describe an N-electron system. Efficiently describing these correlations has been the guiding principle for quantum chemists building approximate methods for solving the full Schrödinger equation. Single reference theories such as coupled-cluster or Møller-Plesset perturbation theories [2, 3, 4] attempt to describe dynamic correlation while multireference theories, such as multiconfigurational self-consistent-field theory, attempt to solve the static correlation problem by extending the SCF procedure to multiple determinants [23].

1.4 Quantum Chemistry For Extended Systems

Quantum chemists have devised a number of efficient methods for solving Schrödinger's equation and the correlation problem of small to medium size molecules and systems. As a result, the properties and spectra of almost any gas phase species can be computed to within chemical accuracy (< 1 kcal/mol). Quantum chemistry can now be used to make spectra prediction for molecular identification, perform geometry optimization for finding ground state conformations, determine transition states for understanding molecular mechanisms, and understand processes like conduction or photo-decomposition. There have been fewer methods developed or adapted to treat phenomena outside of the gas phase. There are numerous puzzles regarding electronic structure of solids, surfaces, and polymers where methods developed in quantum chemistry can provide qualitative and quantitative solutions [13, 12].

Luckily, the first steps extending quantum chemical methods to systems with periodicity have been taken in the form of generalizing the molecular Hartree-Fock procedure to systems with periodic boundaries [15, 8, 9, 12]. This method addresses many of the issues of how to build a translationally invariant basis for a crystal out of atomic orbitals, how to perform infinite lattice summations, and which symmetries must necessarily be obeyed by the Hamil-

tonian [7, 25]. It also connects density functional theory, the computational workhorse of solid-state simulation, with atomic orbital basis sets instead of the plane waves used in most periodic DFT calculations. In many cases, such as metal-oxide insulators, covalently bonded polymers, and zeolites, the electron distributions are spatially localized making them difficult to describe by plane waves and optimally described by local basis set theories developed for quantum chemistry [21]. Most importantly, the crystalline-orbital method is a starting point to treat electron correlation in bulk materials.

1.5 Thesis Outline

In this thesis we will use the variational two-electron reduced density matrix method to capture electron correlation in models of cuprate superconductors and polymers described in atomic orbital basis sets. This will involve generalizing the variational two-electron reduced density matrix method, traditionally used on finite systems with open boundaries, to extended systems with periodic boundaries. In Chapter 2 we will describe the important theoretical and computational aspects of variational 2-RDM theory. In Chapters 3 and 4 we discuss the performance of variational 2-RDM theory and approximate N-representability for describing strong correlation in two model systems. The first is the classic Hubbard model with linear and ladder lattice topologies. The second model is a class of Hamiltonians that have only two-body interactions and is known to contain superconducting correlations. In Chapters 5 and 6 we present a formalism for *ab initio* simulations of bulk materials using atomic orbital basis sets developed for quantum chemistry, and determine the necessary N-representability constraints on the 2-RDM to accurately compute their ground states.

1.6 References

[1] Philip W Anderson. Superconductivity in high tc cuprates: The cause is no longer a mystery. *Physica Scripta*, pages 10–12, 2002.

[2] Rodney J Bartlett. Many-body perturbation theory and coupled cluster theory for electron correlation in molecules. *Ann. Rev. Phys. Chem.*, 32(1):359–401, 1981.

[3] Rodney J Bartlett and Monika Musiał. Coupled-cluster theory in quantum chemistry. *Rev. Mod. Phys.*, 79(1):291, 2007.

[4] T Daniel Crawford and HF Schaefer. An introduction to coupled cluster theory for computational chemists. *Reviews in computational chemistry*, 14:33–136, 2000.

[5] Elbio Dagotto and T. M. Rice. Surprises on the way from one- to two-dimensional quantum magnets: The ladder materials. *Science*, 271(5249):618–623, February 1996.

[6] Ernest R Davidson. The iterative calculation of a few of the lowest eigenvalues and corresponding eigenvectors of large real-symmetric matrices. *J. Comp. Phys.*, 17(1):87–94, 1975.

[7] Joseph Delhalle, Lucjan Piela, Jean-Luc Brédas, and Jean-Marie André. Multipole expansion in tight-binding hartree-fock calculations for infinite model polymers. *Phys. Rev. B*, 22:6254–6267, Dec 1980.

[8] R Dovesi, C Pisani, and C Roetti. Hartree-fock ab initio treatment of crystalline systems. *Lecture Notes in Chemistry*, 48, 1988.

[9] Robert A Evarestov. *Quantum chemistry of solids: the LCAO first principles treatment of crystals*, volume 153. Springer Science & Business Media, 2007.

[10] Gene H Golub and Charles F Van Loan. matrix computations, 3rd ed., 1996.

[11] Trygve Helgaker, Poul Jorgensen, and Jeppe Olsen. *Molecular electronic-structure theory*. John Wiley & Sons, 2014.

[12] So Hirata. Quantum chemistry of macromolecules and solids. *Phys. Chem. Chem. Phys.*, 11:8397–8412, 2009.

[13] Roald Hoffmann. How chemistry and physics meet in the solid state. *Angewandte Chemie International Edition in English*, 26(9):846–878, 1987.

[14] J. Hubbard. Electron correlations in narrow energy bands. *Proc. R. Soc. Lond. A*, 276(1365):238–257, November 1963.

[15] J. Ladik. *Electronic structure of polymers and molecular crystals*, volume 9. Springer Science & Business Media, 2013.

[16] Cornelius Lanczos. *An iteration method for the solution of the eigenvalue problem of linear differential and integral operators*. United States Governm. Press Office, 1950.

[17] N. F. Mott. The basis of the electron theory of metals, with special reference to the transition metals. *Proc. R. Soc. Lond. A*, 62, 1949.

[18] Rudolph Pariser and Robert G Parr. A semi-empirical theory of the electronic spectra and electronic structure of complex unsaturated molecules. i. *J. Chem. Phys.*, 21(3):466–471, 1953.

[19] Rudolph Pariser and Robert G Parr. A semi-empirical theory of the electronic spectra and electronic structure of complex unsaturated molecules. ii. *The Journal of Chemical Physics*, 21(5):767–776, 1953.

[20] Beresford N Parlett. *The symmetric eigenvalue problem*, volume 7. SIAM, 1980.

[21] Cesare Pisani. *Quantum-mechanical ab-initio calculation of the properties of crystalline materials*, volume 67. Springer Science & Business Media, 2012.

[22] J. A. Pople. Electron interaction in unsaturated hydrocarbons. *Trans. Faraday Soc.*, 49:1375–1385, 1953.

[23] Ron Shepard. The multiconfiguration self-consistent field method. *Ab Initio Methods in Quantum Chemistry, KP Lawley, ed*, (2):63, 1987.

[24] Attila Szabo and Neil S Ostlund. *Modern quantum chemistry: introduction to advanced electronic structure theory*. Courier Corporation, 2012.

[25] Hiroyuki Teramae. Study on the behavior of energy convergence in ab initio crystal orbital calculations. *Theo. Chem. Acc.*, 94(6):311–331, 1996.

CHAPTER 2

VARIATIONAL 2-RDM THEORY

2.1 The Reduced Hamiltonian and the 2-Particle Density Matrix

The Full Configuration Interaction problem can be recast as a variational minimization over the cone of N-body positive semidefinite density matrices of unit trace.

$$\min \quad E = \langle \hat{H}, {}^{N}D \rangle \tag{2.1}$$

$$\text{s.t. } \langle I, {}^{N}D \rangle = 1 \;\; {}^{N}D \succeq 0 \tag{2.2}$$

${}^{N}D$ is the outer product of the full N-body wave function producing the von Neumann density matrix.

$${}^{N}D = \psi(1, 2, .., N)\psi(1', 2', .., N')^{*} \tag{2.3}$$

Because the Hamiltonian contains no more than two-electron interactions and electrons are indistinguishable we can express the N-body Hamiltonian as a reduced operator that has only two-electron dependence without loss of information.

$${}^{2}K(12) = N\hat{h}(1) + \frac{N(N-1)}{2}\hat{V}(12) \tag{2.4}$$

Therefore, we no longer need the entire N-body probability distribution of electrons in the von Neumann density matrix to evaluate the expectation value of the Hamiltonian operator. We need only the pairwise electron probability distribution which can be obtained by contraction of the N-body distribution onto the two-particle space [11].

$$E = \langle {}^{2}K, {}^{2}D \rangle \tag{2.5}$$

$$^2D = \int {}^N D \; d3, ..., dN \tag{2.6}$$

By introducing a basis we can express ^2K and ^2D as four index tensors

$$^2K^{k,l}_{i,j} = \frac{1}{N-1}\left(\delta^k_i \hat{h}^l_j \hat{a}^\dagger_l \hat{a}_j - \delta^l_i \hat{h}^k_j \hat{a}^\dagger_k \hat{a}_j - \delta^k_j \hat{h}^l_i \hat{a}^\dagger_l \hat{a}_i + \delta^l_j \hat{h}^k_i \hat{a}^\dagger_k \hat{a}_i\right) + V^{kl}_{ij} \hat{a}^\dagger_k \hat{a}^\dagger_l \hat{a}_j \hat{a}_i \tag{2.7}$$

$$^2D^{k,l}_{i,j} = \mathrm{Tr}[\hat{a}^\dagger_k \hat{a}^\dagger_l \hat{a}_j \hat{a}_i, {}^2D] \tag{2.8}$$

and form a new 2-body minimization problem, Eq. 2.9, that involves a computational object that scales as r^4–where r is the number of one-particle basis functions–instead of the factorial scaling object associated with FCI or optimization over von Neumann density matrices.

$$\min \quad E = \sum_{ijkl} {}^2K^{kl}_{ij} \, {}^2D^{kl}_{ij} \tag{2.9}$$

$$\text{s.t.} \quad {}^2D \succeq 0 \quad \mathrm{Tr}[{}^2D] = \binom{N}{2} \tag{2.10}$$

2.2 N-representability

It was determined by Tredgold and Coleman that free minimization of the energy with respect to the 2-RDM over the 2-cone determined by the von Neumann conditions results in unphysical ground states because the variational space of 2-RDM's is larger than the set of 2-RDM's that can be contracted from a pure or ensemble Fermionic N-particle density matrix [25, 6, 7]. Therefore, the main objective in the N-representability problem is to determine the necessary and sufficient conditions on the two-electron density matrix to ensure it has an N-body preimage–i.e. determining an adequate characterization of the 2-cone [6, 7]. A powerful set of approximate N-representability conditions, which emerge from the constructive solution to the N-representability problem [18], called p-positivity, provide a hierarchy of non-negativity constraints on the eigenvalues of the 2-RDM and its associated

metric matrices [6, 9, 20, 12, 28]. p-positivity restricts the $(p+1)$ metric (or overlap) matrices of the form

$$M = \langle\psi|\hat{C}^\dagger\hat{C}|\psi\rangle \tag{2.11}$$

to be positive semidefinite. The operator $\hat{C}$ represents the set of p-particle operators that form the basis functions from which the overlap matrix is obtained. The 2-positive matrices are generated from the set $\hat{C} = \{\hat{a}_i, \hat{a}_i^\dagger, \hat{a}_i\hat{a}_j, \hat{a}_i^\dagger\hat{a}_j, \hat{a}_i^\dagger\hat{a}_j^\dagger\}$ and produce the following metric matrices.

$$\begin{aligned}
{}^1D_i^j &= \langle\psi|\hat{a}_j^\dagger\hat{a}_i|\psi\rangle \\
{}^1Q_i^j &= \langle\psi|\hat{a}_j\hat{a}_i^\dagger|\psi\rangle \\
{}^2D_{i,j}^{p,q} &= \langle\psi|\hat{a}_p^\dagger\hat{a}_q^\dagger a_j\hat{a}_i|\psi\rangle \\
{}^2Q_{i,j}^{p,q} &= \langle\psi|\hat{a}_p\hat{a}_q\hat{a}_j^\dagger\hat{a}_i^\dagger|\psi\rangle \\
{}^2G_{i,j}^{p,q} &= \langle\psi|\hat{a}_p^\dagger\hat{a}_q\hat{a}_j^\dagger\hat{a}_i|\psi\rangle
\end{aligned} \tag{2.12}$$

The non-negativity of these density matrices correspond with physically restricting the probabilities of finding one-particle, one-hole, two-particles, two-holes, and particle-hole pairs to be non-negative. These matrices contain equivalent information as each matrix can be expressed in a one-to-one mapping of another by the Fermionic anticommutation relations.

$$\{\hat{a}_i^\dagger, \hat{a}_j\} = \hat{a}_i^\dagger\hat{a}_j + \hat{a}_j\hat{a}_i^\dagger = \delta_i^j \tag{2.13}$$

$${}^1D_i^j + {}^1Q_i^j = \delta_i^j \tag{2.14}$$

$$ {}^2Q^{p,q}_{ij}/2 = \left(\delta^p_i - 2\ {}^1D^p_i\right) \wedge \delta^q_j + \ {}^2D^{p,q}_{i,j}/2 \tag{2.15} $$

$$ {}^2G^{k,l}_{ij} = \delta^i_p\ {}^1D^q_j - {}^2\ D^{i,q}_{p,j} \tag{2.16} $$

The equivalency by linear mapping between the metric matrices does not imply the redundancy in characterizing an approximate 2-cone and are necessary constraints in the p-positivity set. Throughout this thesis the 2-positive constraints are denoted by DQG. We can further augment the approximation of the 2-cone if we consider $\{\hat{C}\}$ to include tuples of creation and annihilation operators. Applying Eq. 6.2 we generate the four 3-positive matrices.

$$ {}^3D^{qrs}_{ijk} = \langle\psi|\hat{a}^\dagger_q\hat{a}^\dagger_r\hat{a}^\dagger_s\hat{a}_k\hat{a}_j\hat{a}_i|\psi\rangle \tag{2.17} $$

$$ {}^3E^{qrs}_{ijk} = \langle\psi|\hat{a}^\dagger_q\hat{a}^\dagger_r\hat{a}_s\hat{a}^\dagger_k\hat{a}_j\hat{a}_i|\psi\rangle \tag{2.18} $$

$$ {}^3F^{qrs}_{ijk} = \langle\psi|\hat{a}_q\hat{a}_r\hat{a}^\dagger_s\hat{a}_k\hat{a}^\dagger_j\hat{a}^\dagger_i|\psi\rangle \tag{2.19} $$

$$ {}^3Q^{qrs}_{ijk} = \langle\psi|\hat{a}_q\hat{a}_r\hat{a}_s\hat{a}^\dagger_k\hat{a}^\dagger_j\hat{a}^\dagger_i|\psi\rangle \tag{2.20} $$

Computationally each of these scales as r^6 with the size of the single particle basis. The expense of the 3-positive conditions can be lowered by introducing approximations to their set. Approximate 3-positivity conditions, proposed by Erdahl and Jin [8] and Erdahl and Mazziotti, [20] are combination of 3-positive matrices

$$ T_1 = {}^3\ D + {}^3\ Q \geq 0 \tag{2.21} $$

$$ T_2 = {}^3\ E + {}^3\ F \geq 0 \tag{2.22} $$

so that the new approximate 3-matrix can be constructed exactly from only knowledge of the 2- and 1-RDMs. This results in a considerable reduction in the numerical implementation [20]. Including the T_2 condition with the 2-positive constraints along with the mapping $M(^1D,^1Q,^2D) \rightarrow T_2$ will be the N-representability constraints denoted DQGT throughout this thesis. There are various other classes of constraints on the 2-RDM, but in this thesis we will focus on the performance of the approximate N-representability generated by considering the p-positive set. Because the set DQG and DQGT are approximation to the true constraints on the 2-cone all ground state energies determined by a minimization with respect these constraints are strictly a lower bound to the exact ground state energy of an N-body quantum systems.

2.3 Semidefinite Programming

The direct minimization of the 2-RDM while maintaining the non-negativity of one- and two-particle metric matrices, connected by linear mappings generated from the Fermionic anitcommutation relations, is a type of optimization known as a semidefinite program [13, 26]. Semidefinite programming is the extension of linear programming to matrix variables and has a variety of applications in other areas such as control theory, finance, and circuit design [24, 22, 27]. The primal semidefinite program is mathematically stated as follows

$$\min \ \langle C, X \rangle \tag{2.23}$$

$$\text{s.t} \ \langle A, X \rangle = b \ ; \ X \succeq 0 \tag{2.24}$$

where C is in the space of symmetric matrices ($C \in \mathcal{S}_n$), X is in the space of positive semidefinite matrices ($X \in \mathcal{S}_n^+$), $\langle \cdot, \cdot \rangle$ is defined as the trace inner product $\text{Tr}[C^T, X]$, and b is a vector in $\mathcal{R}^m$. The conjugate dual of the primal problem can be determined in the normal way by considering the maximization of dual variables with an inner minimization

over the primal.

$$\max \; b^T y \tag{2.25}$$

$$\text{s.t} \;\; S = C - y^T A \; ; \; S \succeq 0 \tag{2.26}$$

Two SDP algorithms were employed in the calculations of the subsequent chapters. These algorithms, known as RRSDP and BPSDP, were developed for 2-RDM methods by Mazziotti [14, 13, 15, 16, 19]. They provide a many-orders-of-magnitude increase in computational efficiency over earlier interior-point algorithms employed in 2-RDM calculations [21, 12, 29]. The first method, known as RRSDP, solves the primal problem by factoring the primal variable ensuring non-negativity.

$$X = RR^T \tag{2.27}$$

The factorization transforms the semidefinite program to a non-linear program which is solved via an augmented-Lagrangian (AL) method [3, 4]. The second method, known as the boundary point method (BPSDP), also uses the AL method to solve the SDP but applies it directly to the dual problem. The boundary point method is 10-20 times faster than RRSDP because it does not involve an unconstrained optimization of the augmented Lagrangian.

2.3.1 RRSDP Method

The RRSDP method exploits the AL method for solving the non-linear programming problem produced by factoring the primal variable. The augmented-Lagrangian method balances the penalty method with the Lagrange multiplier method to prevent ill conditioning

as the penalty parameter increases [2, 1]. Considering the augmented-Lagrangian

$$L(R, y, \sigma) = \langle C, RR^T \rangle - \sum_{y=1}^{m} y_i(\langle A_i, RR^T \rangle - b_i) + \frac{\sigma}{2} \sum_{i=1}^{m} (\langle A_i, RR^T \rangle - b_i)^2 \tag{2.28}$$

we seek an optimal primal dual pair $(R^*, (y^*, \sigma^*))$ that minimizes the objective $\langle C, RR^T \rangle$ and satisfies $\langle A_i, RR^T \rangle = b_i$ for all constraints $\{i\}$. One of the main reasons for using the AL is if given (y^*, σ^*) one can determine R^* by simply minimizing $L(\cdot, y^*, \sigma^*)$ with respect to R. We generate the optimal multiplier (y) and penalty (σ) by iteratively determining the sequence (y^k, σ^k) that converges to the solution (y^*, σ^*). The sequence is produced by the following procedure:

I. Minimize $L(\cdot, y, \sigma)$ with respect to R

II. compute $v = ||\langle A, RR^T \rangle - b||_\infty$

III. if $v < \eta v_k$, set

$$y_i^{k+1} = y_i^k - \sigma_k(\langle A_i, RR^T \rangle - b_i) \tag{2.29}$$

$$\sigma_{k+1} = \sigma_k \tag{2.30}$$

$$v_{k+1} = v \tag{2.31}$$

IV. else,

$$y_i^{k+1} = y_i \tag{2.32}$$

$$\sigma_{k+1} = \gamma \sigma_k \tag{2.33}$$

$$v_{k+1} = v_k \tag{2.34}$$

The outlined procedure is repeated until primal and dual feasibility are below a particular threshold (ϵ). For the dual multiplier and penalty update steps, the variable η certifies that there has been a sufficient decrease in the primal feasibility while γ increases the penalty parameter in an attempt to bias the AL problem to the solution. Each minimization of the AL is computed using the low-memory BFGS procedure [5] which requires the value of the AL and it's derivative.

$$\nabla_R L(R, y, \sigma) = 2\overline{S}R \tag{2.35}$$

$$\overline{S} = C - \sum_{i=1}^{m} \Big(y_i - \sigma(\langle A_i, RR^T \rangle - b_i) \Big) A_i \tag{2.36}$$

It is clear that the update for the Lagrange multipliers ensures the next iteration will be dual feasible for the unaugmented Lagrangian. As with most multiplier methods there are various ways to perform the multiplier updates. In the conclusion chapter of this thesis we discuss a new method for updating (y) which includes second order information.

2.3.2 BPSDP Method

The boundary point method also exploits the AL form of the SDP but applies it to the dual problem [23].

$$L(y, S, X) = b^T y + \langle X, S + C - A^T y \rangle + \frac{\sigma}{2} ||S + C - A^T y||^2 \tag{2.37}$$

The augmented-lagrangian is minimized to determine an optimal (y, S), where $S \succeq 0$, with fixed primal variable X. The primal variable is then updated in a first-order step.

$$X_{k+1} = X_k + \sigma(S + C - A^T y) \tag{2.38}$$

This procedure is continued until dual feasibility is reached or below a particular threshold $||S + C - A^T y|| < \epsilon$. The key innovation in the algorithm is determining the minimizer of the augmented-Lagrangian. Povh *et. al.* first re-write the augmented Lagrangian by first defining $W(y)$

$$W(y) = A^T y - C - \frac{1}{\sigma} X \tag{2.39}$$

the AL becomes

$$L_\sigma = b^T y + \frac{\sigma}{2}||S - W(y)||^2 - \frac{1}{2\sigma}||X||^2 \tag{2.40}$$

Clearly, minimizing the AL with respect to (y, S) will only involve the first two terms of the rewritten AL. This "inner" minimization is a quadratic SDP problem that is solved iteratively. By first introducing the Lagrange multiplier $V \succeq 0$ for the inner minimization problem we get the following Lagrangian.

$$L(y, S; V) = b^T y + \frac{\sigma}{2}||S - W(y)||^2 - \langle V, S \rangle \tag{2.41}$$

The solution to this problem is determined in the usual manner by considering the KKT conditions on the Lagrangian.

$$A(A^T y) = A(S + C + \frac{1}{\sigma} X) - \frac{1}{\sigma} b \tag{2.42}$$

$$V = \sigma S - \sigma W(y) \tag{2.43}$$

Povh *et. al.* noticed that when minimizing the Lagrangian in Eq. 2.41 if y is kept fixed then S is the projection onto the cone of positive-semidefinite matrices. Determining the closest positive semidefinite matrix is equivalent to partitioning positive and negative eigenvalues and eigenvectors [10]. Thus the inner optimization is performed by first solving a system

of equations for multipliers y and then performing an eigenvalue decomposition for the projection onto the positive semidefinite cone in order to maintaining $S \succeq 0$. The total boundary point algorithm is as follows

I. minimize outer Lagrangian; repeat until $\delta_{\text{outer}} < \epsilon_{\text{outer}}$

   A. minimize inner Lagrangian; repeat until $\delta_{\text{inner}} < \epsilon_{\text{inner}}$

      1. solve for y^k: $A(A^T y) = A(S^k + C + \frac{1}{\sigma} X^k) - \frac{1}{\sigma} b$
      2. Positive projection step: $W = A^T y^k - C - \frac{1}{\sigma} X^k$; $S^k = W_+$; $V^k = W_-$
      3. $\delta_{\text{inner}} = ||\langle A, V^k \rangle - b||$

II. $X^{k+1} = V^k$

III. $k = k + 1$; $\delta_{\text{outer}} = ||S^k - A^T y^k + C||$

IV. update σ

Here the positive and negative projections W_+ and W_- are determined by the minimization

$$W_+ = \text{argmin}_{U \succeq 0} ||W - U|| \tag{2.44}$$

which corresponds to generating the W_+ by an eigenvalue decomposition and selecting positive eigenvalues along with their associated eigenvectors.

$$W_+ = \sum_i \lambda_i^+ |\phi_i\rangle\langle\phi_i| \quad W_- = \sum_j \lambda_j^- |\phi_j\rangle\langle\phi_j| \tag{2.45}$$

The computationally expensive task is the determination of y in the inner minimization problem. As AA^T does not change its Cholesky decomposition can be formed prior to the calculation and then used to back-solve for y^k. This lack of unconstrained minimization is the reason for the 10-20 times speed increase of BPSDP over RRSDP. Though convergence is guaranteed for any penalty parameter we can accelerate convergence by dynamically

updating σ. This is accomplished by setting σ according to primal and dual feasibility [17].

$$\sigma = \sigma\delta_{\text{outer}}/\delta_{\text{inner}} \tag{2.46}$$

2.4 References

[1] Dimitri P Bertsekas. Multiplier methods: a survey. *Automatica*, 12(2):133–145, 1976.

[2] Dimitri P Bertsekas. *Constrained optimization and Lagrange multiplier methods*. Academic press, 2014.

[3] Samuel Burer and Renato DC Monteiro. A nonlinear programming algorithm for solving semidefinite programs via low-rank factorization. *Mathematical Programming*, 95(2):329–357, 2003.

[4] Samuel Burer and Renato DC Monteiro. Local minima and convergence in low-rank semidefinite programming. *Mathematical Programming*, 103(3):427–444, 2005.

[5] Richard H Byrd, Jorge Nocedal, and Robert B Schnabel. Representations of quasi-newton matrices and their use in limited memory methods. *Mathematical Programming*, 63(1-3):129–156, 1994.

[6] A. J. Coleman. Structure of fermion density matrices. *Rev. Mod. Phys.*, 35:668–686, Jul 1963.

[7] A. John Coleman. *Reduced density matrices:Coulson's challenge*. Springer, 2000.

[8] R. M. Erdahl. *Int. J. Quantum Chem*, 13, 1978.

[9] Claude Garrod and Jerome K. Percus. Reduction of the n-particle variational problem. *J. Math. Phys.*, 5(12):1756–1776, 1964.

[10] Nicholas J Higham. Computing a nearest symmetric positive semidefinite matrix. *Linear algebra and its applications*, 103:103–118, 1988.

[11] Hans Kummer. n-representability problem for reduced density matrices. *J. Math. Phys.*, 8:2063 – 2082, 1967.

[12] David A. Mazziotti. Variational minimization of atomic and molecular ground-state energies via the two-particle reduced density matrix. *Phys. Rev. A*, 65:062511, Jun 2002.

[13] David A. Mazziotti. First-order semidefinite programming for the direct determination of two-electron reduced density matrices with application to many-electron atoms and molecules. *J. Chem. Phys.*, 121(22):10957–10966, 2004.

[14] David A. Mazziotti. Realization of quantum chemistry without wave functions through first-order semidefinite programming. *Phys. Rev. Lett.*, 93:213001, Nov 2004.

[15] David A Mazziotti. *Advances in Chemical Physics, Reduced-Density-Matrix Mechanics: With Application to Many-Electron Atoms and Molecules*, volume 134. John Wiley & Sons, 2007.

[16] David A. Mazziotti. Large-scale semidefinite programming for many-electron quantum mechanics. *Phys. Rev. Lett.*, 106:083001, Feb 2011.

[17] David A Mazziotti. Large-scale semidefinite programming for many-electron quantum mechanics. *Phys. Rev. Lett.*, 106(8):083001, 2011.

[18] David A. Mazziotti. Structure of fermionic density matrices: Complete n-representability conditions. *Phys. Rev. Lett.*, 108:263002, Jun 2012.

[19] David A. Mazziotti. Two-electron reduced density matrix as the basic variable in many-

electron quantum chemistry and physics. *Chemical Reviews*, 112(1):244–262, 2012. PMID: 21863900.

[20] David A. Mazziotti and Robert M. Erdahl. Uncertainty relations and reduced density matrices: Mapping many-body quantum mechanics onto four particles. *Phys. Rev. A*, 63:042113, Mar 2001.

[21] Maho Nakata, Hiroshi Nakatsuji, Masahiro Ehara, Mitsuhiro Fukuda, Kazuhide Nakata, and Katsuki Fujisawa. Variational calculations of fermion second-order reduced density matrices by semidefinite programming algorithm. *Journal of Chemical Physics*, 114(19):8282–8292, 2001.

[22] Yurii Nesterov, Arkadii Nemirovskii, and Yinyu Ye. *Interior-point polynomial algorithms in convex programming*, volume 13. SIAM, 1994.

[23] Janez Povh, Franz Rendl, and Angelika Wiegele. A boundary point method to solve semidefinite programs. *Computing*, 78(3):277–286, 2006.

[24] Jos F Sturm. Using sedumi 1.02, a matlab toolbox for optimization over symmetric cones. *Optimization methods and software*, 11(1-4):625–653, 1999.

[25] R. H. Tredgold. Density matrix and the many-body problem. *Phys. Rev.*, 105:1421–1423, Mar 1957.

[26] Lieven Vandenberghe and Stephen Boyd. Semidefinite programming. *SIAM review*, 38(1):49–95, 1996.

[27] Lieven Vandenberghe and Stephen Boyd. Applications of semidefinite programming. *Applied Numerical Mathematics*, 29(3):283–299, 1999.

[28] Zhengji Zhao, Bastiaan J. Braams, Mituhiro Fukuda, Michael L. Overton, and Jerome K. Percus. The reduced density matrix method for electronic structure cal-

culations and the role of three-index representability conditions. *J. Chem. Phys.*, 120(5):2095–2104, 2004.

[29] Zhengji Zhao, Bastiaan J Braams, Mituhiro Fukuda, Michael L Overton, and Jerome K Percus. The reduced density matrix method for electronic structure calculations and the role of three-index representability conditions. *The Journal of chemical physics*, 120(5):2095–2104, 2004.

CHAPTER 3

COMPARISON OF ONE-DIMENSIONAL AND QUASI-ONE-DIMENSIONAL HUBBARD MODELS FROM THE VARIATIONAL TWO-ELECTRON REDUCED-DENSITY-MATRIX METHOD

3.1 High-Temperature Superconductivity and Lattice models

The study of superconducting phenomenon is vast and a highly active field. Since the discovery of superconductivity in Mercury (Hg), with a T_c of 4.19 K, many other materials with significantly higher transition temperature have been discovered. Until 1986 when the first high-temperature superconducting (HTSC) material was found by Berdnorz and Müller [6] it was widely accepted that the theory of Bardeen, Cooper and, Schieffer (BCS) which stated that electrons condensed into coherent pairs from electron-phonon interactions was responsible for superconductivity [5].

Since the discovery of HTSC other compounds belonging to the same class of cuperate structures have been found with even higher superconducting transition temperatures [15, 38]. The puzzling nature of this class of materials is the lack of an appreciable electron-phonon interaction that could lead to significantly higher T_c. A theoretical description of the endogenous mechanism for superconductivity has yet to be elucidated. During the search for a SC mechanism experimentalists and theorists have determined some prominent features the HTSC cuperate class: i) the commonality of a Cu-O plane within HTSC materials strongly suggests that the principle locus of superconductivity is the Cu-O planes, ii) inter-plane interaction is weak relative to $k_\beta T_c$ iii) the spin-state of the pairs is a singlet iv) and the

spatial symmetry is B_{1g} ($d_{x^2-y^2}$) of the C_4v or D_4h groups [24].

There are many proposed single, and multiband, models for HTSC phenomenon [11, 4], predominantly of the t-J or Hubbard model type in two, or quasi-two-dimensions. The t-J and Hubbard type interactions are chosen because they are the simplest descriptors of antiferromagnetic ground states which are the striking feature of all undoped cuperate parent compounds. In fact, Allen put forth the Hubbard-hypothesis stating

The fundamental physics of the oxide superconductors is contained in the [Hubbard] Hamiltonian on a square lattice for a small number of holes [1]

As of yet there is no clear consensus on the mechanism for how superconductivity arrises or if the Hubbard model provides the necessary interaction types to sustain a SC state on a one- or two-dimensional lattice. Keeping this in mind guides the next two chapters.

3.2 Overview

We examine the electron correlation of one-dimensional and quasi-one-dimensional Hubbard models with two sets of approximate N-representability conditions. While recent RDM calculations have examined linear[19] as well as 4×4 and 6×6 Hubbard lattices,[2, 35] there has not been an exploration of RDMs on quasi-one-dimensional Hubbard lattices with a comparison to the one-dimensional Hubbard lattices. How does the electron correlation change as we move from a one-dimensional to a quasi-one-dimensional Hubbard model? How are these changes in correlation reflected in the required N-representability conditions on the 2-RDM? One- and two-particle correlation functions are used to compare the electronic structure of the half-filled states of the 1×10 and 2×10 lattices with periodic boundary conditions. The degree of correlation captured by approximate N-representability conditions is probed by examining the 1-particle occupations around the Fermi surfaces of both lattices and measuring the entanglement with a size-extensive correlation metric, the Frobenius norm squared of the cumulant part of the 2-RDM.[22]

3.3 Model

The single-band ladder extension of the one-dimensional Hubbard model [21, 18, 17] has been utilized as a minimalist model to study spin-liquid behavior[14, 29, 12] and high-temperature superconductors.[3, 20, 7, 30, 23] The ladder model is a quasi-one-dimensional system with a four-fold degenerate Fermi surface and correlations in two-dimensions.

3.3.1 Hamiltonian

The Hamiltonian of the ladder single-band model in position space is defined as follows:

$$\hat{H} = \quad t \sum_{n,\lambda,\sigma} (\hat{a}^{\dagger}_{n,\lambda,\sigma} \hat{a}_{n+1,\lambda,\sigma} + \hat{a}^{\dagger}_{n+1,\lambda,\sigma} \hat{a}_{n,\lambda,\sigma}) \tag{3.1}$$

$$+ \quad t_{\perp} \sum_{n,\sigma} (\hat{a}^{\dagger}_{n,a,\sigma} \hat{a}_{n,b,\sigma} + \hat{a}^{\dagger}_{n,b,\sigma} \hat{a}_{n,a,\sigma}) \tag{3.2}$$

$$+ \quad U \sum_{n} \hat{a}^{\dagger}_{n,\lambda,\sigma} \hat{a}_{n,\lambda,\sigma} \hat{a}^{\dagger}_{n,\lambda,-\sigma} \hat{a}_{n,\lambda,-\sigma} \tag{3.3}$$

where t is a parameter controlling transport between rungs of the ladder, $t_{\perp}$ is a parameter controlling transport between the two sides of a ladder's rung, U is a parameter controlling the one-site repulsion between electrons, the index n is the rung number, the index $\lambda = a(b)$ corresponds to a ladder leg, and the index σ indicates the spin of the electron created at rung n on leg $a(b)$. We impose periodic boundary conditions along the legs of the ladder forming a Hubbard ribbon.

3.3.2 Spin and Spatial Symmetry Adaptation

One can take advantage of any spin or spatial symmetry in the Hamiltonian by symmetry adapting the metric matrices and thereby reducing the size of the 2-RDM to be optimized.[16] For the ladder model we transform the RDMs to bonding and antibonding spaces and then Fourier transform to take advantage of the translational symmetry. We consider linear com-

bination of creation and annihilation operators to form two disjoint one-electron subspaces

$$\hat{a}^B_{n,\sigma} = \frac{1}{\sqrt{2}}\left(\hat{a}_{n,a,\sigma} + \hat{a}_{n,b,\sigma}\right) \tag{3.4}$$

$$\hat{a}^A_{n,\sigma} = \frac{1}{\sqrt{2}}\left(\hat{a}_{n,a,\sigma} - \hat{a}_{n,b,\sigma}\right), \tag{3.5}$$

where $\hat{a}^B_{n,\sigma}$ and $\hat{a}^A_{n,\sigma}$ are annihilation operators for the bonding and antibonding orbitals with spin $\sigma \in \{\alpha, \beta\}$. The one-body part of the Hamiltonian divides into anti-bonding $\hat{H}_A$ and bonding $\hat{H}_B$ parts:

$$\hat{H} = \hat{H}_A + \hat{H}_B + \hat{H}^{AB}_{\text{int}}. \tag{3.6}$$

When expressed in the bonding and antibonding basis, the interaction term decomposes into four two-body operators representing inter- and intra-subspace pair scattering and inter- and intra-subspace pair exchange.

Spatial symmetry is imposed in each one-electron space by the Bloch transformation

$${}^B\hat{a}_{n,\sigma} = \frac{1}{\sqrt{N_x}}\sum_{k_b} e^{-ik_b n}\hat{a}_{k_b,\sigma} \tag{3.7}$$

$${}^A\hat{a}_{n,\sigma} = \frac{1}{\sqrt{N_x}}\sum_{k_a} e^{-ik_a n}\hat{a}_{k_a,\sigma}, \tag{3.8}$$

where $\hat{a}_{k_b,\sigma}$ annihilates an electron with momentum k_b in the bonding band and $\hat{a}_{k_a,\sigma}$ annihilates an electron with momentum k_a in the antibonding band. The Hamiltonian and 2-RDM can also be spin adapted. As discussed in Ref. [16], because the three triplet blocks are equivalent in the singlet case, each metric matrix has only two distinct spin blocks defined by the folded operators

$$\hat{C}^{0,0}_{i,j;i\leq j} = \frac{1}{\sqrt{2}}(\hat{a}^\dagger_{i,\alpha}\hat{a}^\dagger_{j,\beta} + \hat{a}^\dagger_{j,\alpha}\hat{a}^\dagger_{i,\beta}) \tag{3.9}$$

$$\hat{C}^{1,0}_{i,j;i<j} = \frac{1}{\sqrt{2}}(\hat{a}^\dagger_{i,\alpha}\hat{a}^\dagger_{j,\beta} + \hat{a}^\dagger_{j,\alpha}\hat{a}^\dagger_{i,\beta}). \tag{3.10}$$

These new $\hat{C}$ operators generate symmetric and antisymmetric parts of ${}^2D$ and ${}^2Q$. Spin-symmetry adaptation of ${}^2G$ and T_2 can be achieved by the same methodology.[28] The size of the 2-RDM can be further reduced by additional symmetries,[37, 35, 13] but they have not been exploited in the present calculations.

3.4 Results

In section 3.4.1 we compare the ground-state energies of the 2×4 ladder system at and below half filling from the variational 2-RDM method with those from full configuration interaction (FCI). Section 3.4.2 contains the analysis of the 2×10 and 1×10 lattices through the α, β-two-point pair correlation function, a measure of one-particle effective hopping, one-electron natural occupation numbers, and the squared Frobenius norm of the cumulant (connected) part of the 2-RDM. Results from 2-RDM calculations with DQG and DQGT conditions are compared.

3.4.1 Energies of Hubbard Ladder

We report the errors in the ground-state energies from the variational 2-RDM method for the 2×4 ladder Hubbard model for a range of interaction strengths where $t = t_\perp = 1$ a.u. Comparisons are made to the ground-state energies from full configuration interaction (FCI). The FCI calculation determines the ground-state energies by computing the lowest eigenvalue of the N-electron Hamiltonian matrix in the basis of all possible Slater determinants. In the FCI calculation the spin orbitals are products of a spin function (α or β) and a "spatial" orbital which can be defined either in the position representation or in the momentum representation. All 2-RDM alculations were optimized until the primal feasibility norm was below 1.0×10^{-5} and the primal-dual gap was below 1.0×10^{-4}. In Fig. 3.1 the error in the ground-state energy and the percentage of the correlation energy recovered from the 2-RDM method with DQG and DQGT conditions is reported for (a) $\langle \hat{n} \rangle = 1$ and (b)

$\langle \hat{n} \rangle = 3/4$ fillings. In the case of half-filling the DQG and the DQGT energies deviate at most from those from FCI by -0.74 a.u. and -0.087 a.u., respectively. The maximum deviations occur in the intermediate interaction regime $U \in [4, 8]$ where there is a large degree of competition between delocalization and localization. For the $\langle \hat{n} \rangle = 3/4$ filling the DQG and DQGT conditions result in a larger absolute error than all corresponding values at half filling, which is consistent with previous observations in the literature[36] that correlated systems with an imbalance between the number of particles and holes require more stringent N-representability constraints.

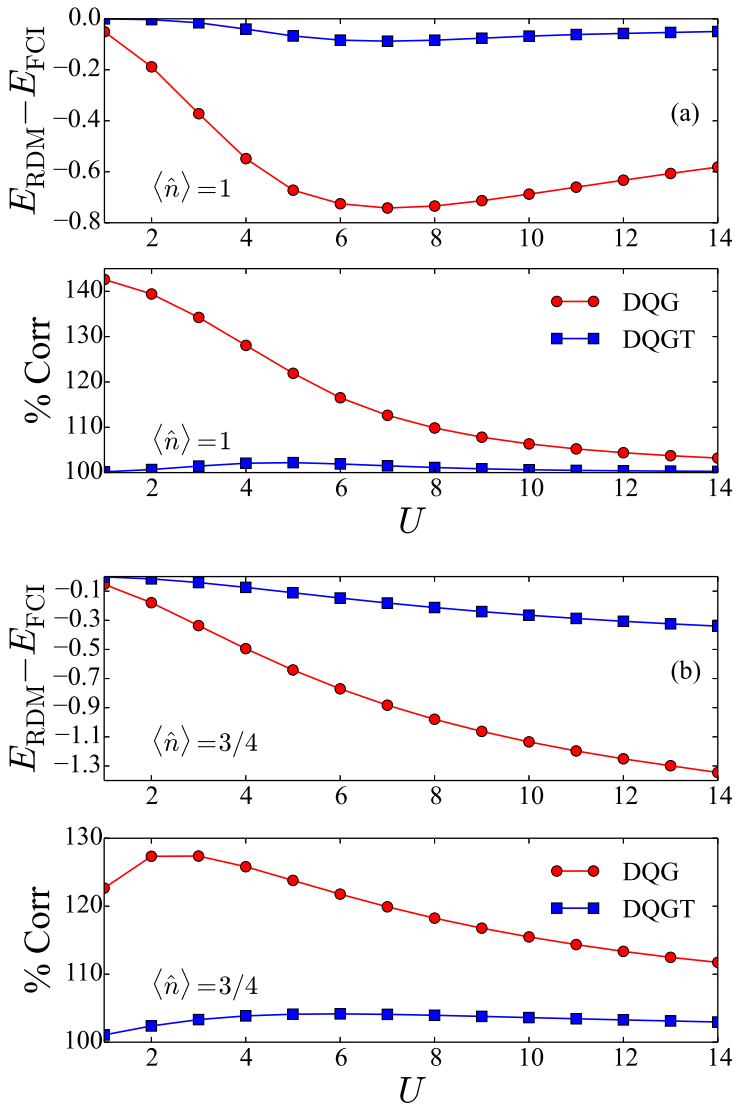

Figure 3.1: Absolute deviation of ground-state energy of the variational 2-RDM method with DQG and DQGT constraints and the percent correlation defined as $(E_{\mathrm{RDM}} - E_{\mathrm{HF}})/(E_{\mathrm{FCI}} - E_{\mathrm{HF}}) \times 100$ are shown for 2×4 lattices at (a) $\langle \hat{n} \rangle = 1$ and (b) $\langle \hat{n} \rangle = 3/4$.

The 2-RDM can be expressed as the wedge product of 1-RDMs (unconnected) plus a cumulant (connected) part[26, 25] denoted as ${}^2\Delta$

$$ {}^2D = {}^1D \wedge {}^1D + {}^2\Delta, \tag{3.11} $$

where the $\wedge$ is the Grassmann wedge product [34, 10, 27]. The unconnected term captures the statistically independent part of the electron pair probability. The energies from the unconnected and connected components[19] are

$$E_1 = \mathrm{Tr}[{}^2K\ ({}^1D \wedge {}^1D)] \tag{3.12}$$

$$E_2 = \mathrm{Tr}[{}^2K\ {}^2\Delta]. \tag{3.13}$$

These energies as well as the Hartree-Fock mean-field energy are plotted in Fig. 3.2. The Hartree-Fock energy grows linearly as U is increased which is closely mirrored by the unconnected piece. Consequently, all the correlated information of the 2-RDM that results in localization is contained in its connected part.

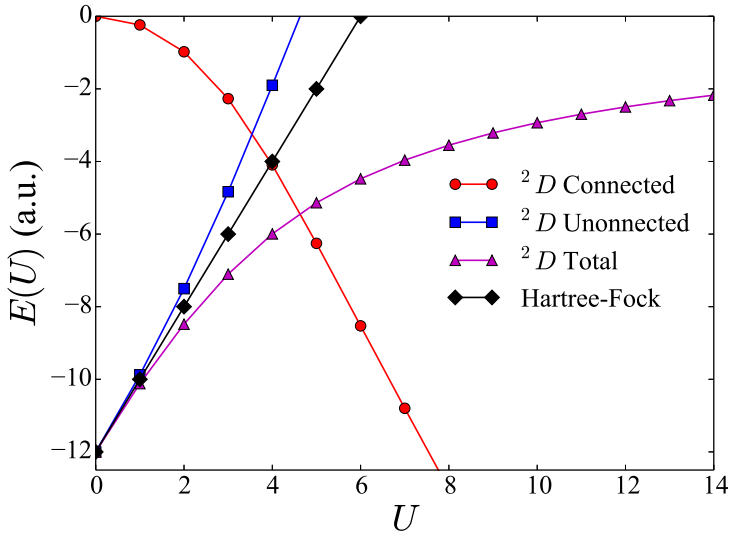

Figure 3.2: For the 2×4 lattice at $\langle \hat{n} \rangle = 1$ the connected, unconnected, and total energies from the variational 2-RDM method with DQGT constraints as well as the Hartree-Fock total energies are shown.

3.4.2 One- and Two-particle Correlations

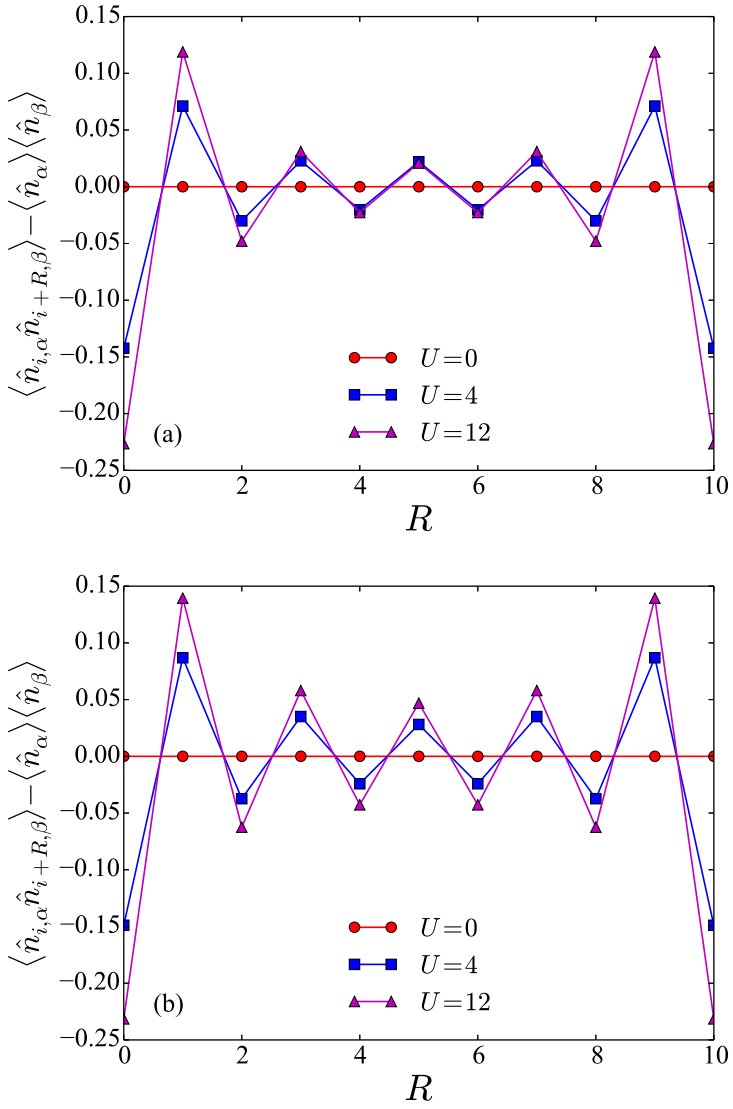

Figure 3.3: The α, β-two-point pair correlation functions of the (a) 2×10 and (b) 1×10 lattices at half filling are computed as a function of R from the variational 2-RDM method with DQGT where R is the distance along each Hubbard strand between the pairs. Because of the periodic boundary conditions, the correlation function values are unique until the lattice inversion center at $R = 5$.

The α, β-two-point pair correlation function for the 2×10 and 1×10 lattices is examined at half filling to explore the variational 2-RDM method with DQG and DQGT conditions. We can express the two point spin-up, spin-down correlation as

$$\langle \hat{n}_{i\alpha} \hat{n}_{i+R\beta} \rangle - \langle \hat{n}_{\alpha} \rangle \langle \hat{n}_{\beta} \rangle, \tag{3.14}$$

where $\langle \hat{n}_{\alpha} \rangle$ is the total density of α-electrons in the system

$$\langle \hat{n}_{\alpha} \rangle = N_{\alpha}/(2N_L), \langle \hat{n}_{\beta} \rangle = N_{\alpha}/(2N_L). \tag{3.15}$$

This correlation function is an extension of the local double-occupancy, $\langle \hat{n}_{i,\alpha} \hat{n}_{i,\beta} \rangle$, which has been used to examine the Mott transition of the Hubbard model defined on various lattices and temperatures. [31, 8, 9, 39]

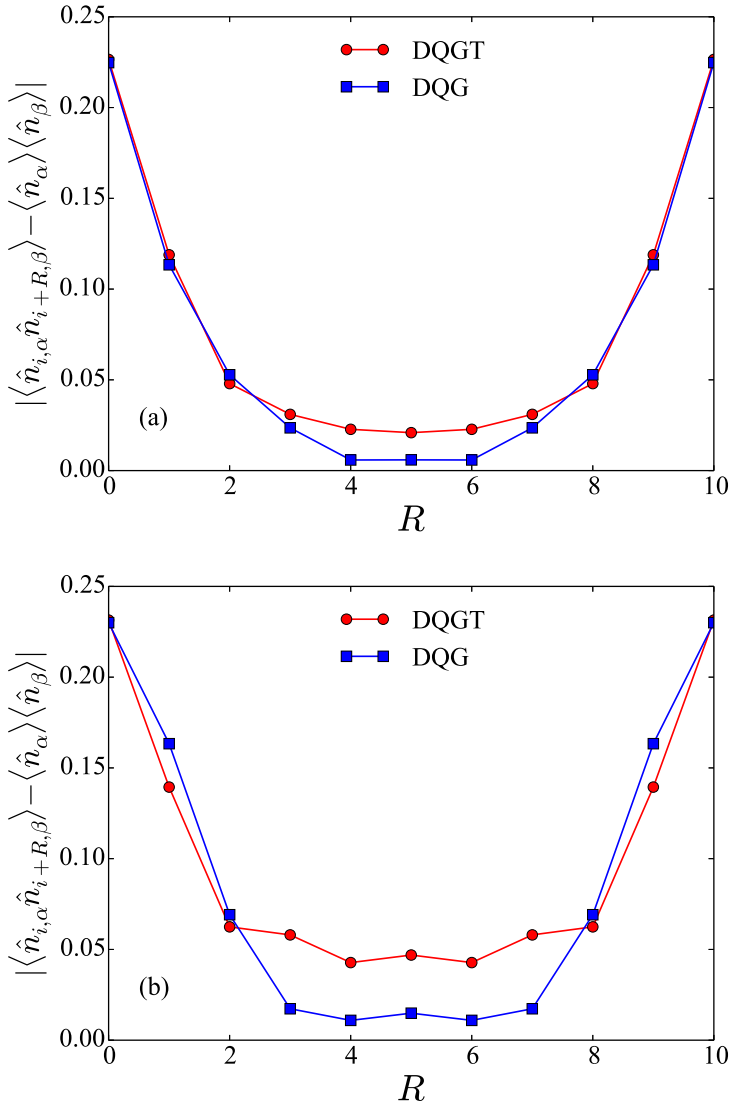

Figure 3.4: The α, β-two-point pair correlation functions calculated with DQG and DQGT constraints are given for the (a) ladder 2×10 and (b) linear 1×10 lattices at half filling $\langle \hat{n} \rangle = 1$.

The pair-correlation function probes the expectation of an antiferromagnetic pair R-sites away from each other in the long direction of the lattice. In the $U = 0$ limit where the α and β electrons are delocalized across the lattice the correlation function is zero for all values of R. As U is increased, antiferromagnetic pairing becomes less favorable and order

is induced. In Figs. 3.3a and 3.3b we plot the two-particle correlation function as a function of R for representative U values. The correlation function decays across the lattice until the inversion center is reached. An exponential fitting of the absolute value of the pair correlation function, not shown, indicates that DQGT predicts a similar decay on the one-dimensional and quasi-one-dimensional lattices. In Fig. 3.4 we plot the absolute value of the pair-correlation function for $U = 12$ from DQG and DQGT to study the differences generated in the (a) ladder and (b) linear lattices from approximate N-representability conditions. In the ladder case the results from DQG and DQGT are in fairly close agreement while in the linear case DQG deviates significantly from DQGT.

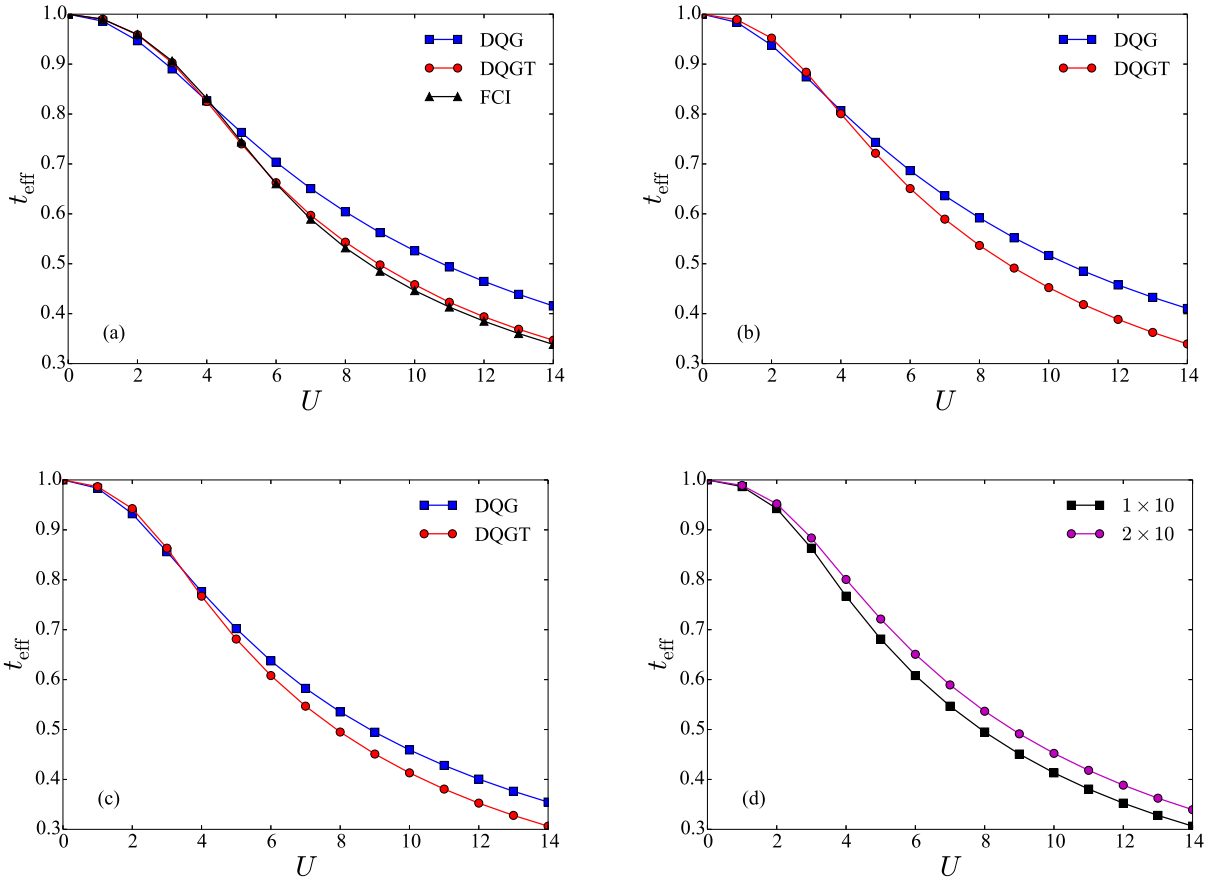

Figure 3.5: The effective hopping t_{eff} for the 2×4 lattice is calculated with DQG, DQGT, and FCI. In (a) we plot t_{eff} for the 2×4 lattice calculated with DQG and DQGT compared against t_{eff} from FCI. We compare t_{eff} from DQG and DQGT for the (b) 2×10 and (c) 1×10 lattices. Both the linear and ladder Hubbard models exhibit the same underestimation of t_{eff} at low U and overestimation of t_{eff} at high U. Part (d) compares t_{eff} calculated from DQGT for the linear and ladder models. The increase in lattice dimension facilitates transport down the chain.

We can use the effective hopping as a one-particle correlation function. Defined in Eq. (3.16), the effective hopping is the likelihood of transport normalized by the non-

interacting limit of the model

$$t_{\text{eff}} = \frac{\langle \hat{a}^\dagger_{i\sigma}\hat{a}_{j\sigma} + \hat{a}^\dagger_{j\sigma}\hat{a}_{i\sigma}\rangle_U}{\langle \hat{a}^\dagger_{i\sigma}\hat{a}_{j\sigma} + \hat{a}^\dagger_{j\sigma}\hat{a}_{i\sigma}\rangle_{U=0}}. \tag{3.16}$$

For low U, where the kinetic energy has the largest energy contribution, approximate N-representability conditions underestimate the effective hopping (kinetic energy), and at high U, where the repulsive interaction term dominates, approximate N-representability conditions underestimate the localization, which causes the effective hopping to be overestimated. In Fig. 3.5a we plot t_{eff} for the 2×4 lattice calculated with DQG and DQGT compared against t_{eff} from FCI. As expected DQG yields a lower t_{eff} than FCI before $U = 4$ and a higher t_{eff} than FCI after $U = 4$. The effective hopping from DQGT shows a similar trend while exhibiting a much smaller deviation from the FCI curve, which reinforces the accuracy of the DQGT conditions for lattices with strongly correlated electrons. We compare t_{eff} from DQG and DQGT for the (b) 2×10 and (c) 1×10 lattices. Both the linear and ladder Hubbard models exhibit the same underestimation of t_{eff} at low U and overestimation of t_{eff} at high U. Figure 3.5d compares t_{eff} calculated from DQGT for the linear and ladder models. The increase in lattice dimension facilitates transport down the chain.

3.4.3 Natural Occupation Numbers and Entanglement

We examine the one-electron occupation numbers of the natural orbitals around the Fermi surface. The natural orbitals are the eigenfunctions of the 1-RDM. Select occupation numbers of the α-spin block of the 1-RDM in the quasi-momentum basis are provided in Table 4.2. For both lattices the $N_\alpha - 1$ and N_α occupation numbers calculated with DQG are larger than the occupation numbers with DQGT, and the $N_\alpha + 1$ and $N_\alpha + 2$ occupation numbers calculated with DQG are smaller than the occupation numbers with DQGT. The difference between DQG and DQGT occupation numbers is greater for the 2×10 lattice than

1×10 lattice for all U values. Furthermore, the higher degree of multireference character of the occupation numbers when calculated with DQGT constraints indicates that polyradical character induced by a transition to the Mott-insulating state is better captured by DQGT conditions.

Table 3.1: Natural-orbital occupation numbers of the α-spin block of the 1-RDM in the quasi-momentum basis.

Lattice	Conditions	U	$N_\alpha - 1$	N_α	$N_\alpha + 1$	$N_\alpha + 2$
1×10	DQG	4	0.9022	0.8064	0.1936	0.0978
		8	0.7828	0.6566	0.3434	0.2172
		12	0.7114	0.6014	0.3986	0.2886
	DQGT	4	0.8993	0.7895	0.2104	0.1008
		8	0.7634	0.6291	0.3710	0.2366
		12	0.6870	0.5812	0.4188	0.3130
2×10	DQG	4	0.8081	0.7667	0.2333	0.1919
		8	0.6629	0.6280	0.3720	0.3371
		12	0.6067	0.5827	0.4173	0.3933
	DQGT	4	0.7863	0.6897	0.3103	0.2138
		8	0.6338	0.5710	0.4290	0.3662
		12	0.5811	0.5462	0.4538	0.4189

We measure correlation explicitly by calculating the squared Frobenius norm of the cumulant portion of the 2-RDM ${}^2\Delta$

$$||{}^2\Delta||^2 = \mathrm{Tr}({}^2\Delta^\dagger \, {}^2\Delta) \tag{3.17}$$

as a function of system size and coupling. The squared Frobenius norm of the cumulant[22] is size-extensive and contains spin entanglement information not captured by the correlation energy or von Neumann entropy. Using this metric, we compare the degree of correlation in each ladder system. In Fig. 3.6 we plot the norm-per-lattice site for the (a) 2×10 and (b) 1×10 lattices at half filling. For the 2×10 lattice DQG predicts a significantly larger norm at high U. In the case of the 1×10 lattice DQG and DQGT agree on the amount of correlation in the lattice.

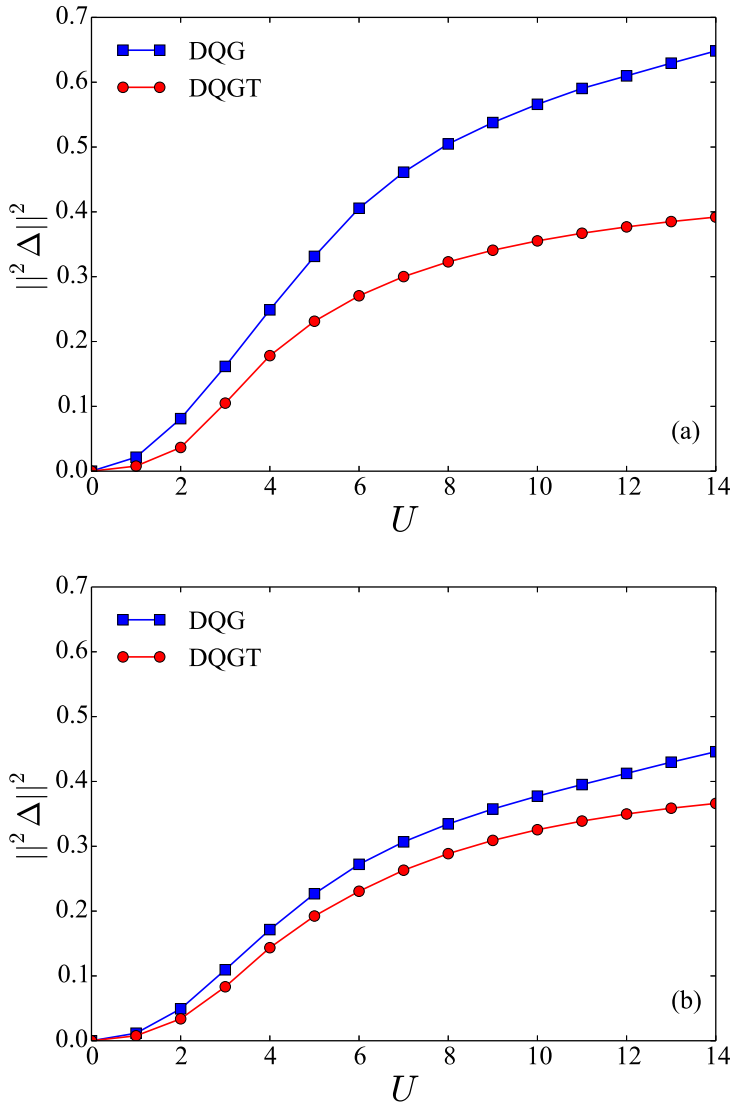

Figure 3.6: Frobenius norm squared of the cumulant part of the 2-RDM is shown for the (a) 2×10 and (b) 1×10 lattices where the 2-RDMs are computed with variational 2-RDM calculations with DQG and DQGT conditions.

3.5 Conclusion

Calculation of ground-state properties of strongly correlated model systems is highly important for understanding a plethora of condensed phase N-body physics. One of the main limitations of wave function methodologies is the exponential scaling of the Hilbert space with system size. In exchange for the exponentially scaling N-particle wave function we have reviewed how to compute the ground-state energy with respect to the polynomial scaling 2-RDM. The variational 2-RDM has some key benefits: (*i*) it provides a lower bound to wave function methods, (*ii*) can be numerically implemented as a semidefinite program which is solved with a polynomial scaling algorithm, and (*iii*) and gives easy access to pair correlation functions important for characterizing condensed-matter systems.

We have demonstrated that the variational 2-RDM method with moderate N-representability constraints can be used to calculate the ground state energies of ladder Hubbard models accurately. In keeping with recent results for 4×4 and 6×6 two-dimensional Hubbard models, we observe that partial (2,3)-positivity (DQGT) conditions are effective at capturing strong electron correlation effects in both one- and quasi-one-dimensional lattices for both half filling and less-than-half filling. We have found that certain correlation functions can be accurately predicted with (2,2)-positivity (DQG) conditions. Furthermore, 2-RDM methods offer a way to analyze the correlation per site in a lattice model with a size-extensive metric and give direct access to occupation numbers. The 2-RDM methods complement recently developed wave-function-based methods [32], and they may be useful in the context of approximate embedding calculations.[33] In general, the variational RDM method offers a new approach to studying lattice models of varying topology and filling.

3.6 References

[1] Philip B Allen, FD Bedard, D Belitz, JE Crow, RA Ferrell, JW Lynn, N Ong, A Santoro, RN Shelton, CS Wang, et al. *High temperature superconductivity*. Springer Science & Business Media, 2012.

[2] James S.M. Anderson, Maho Nakata, Ryo Igarashi, Katsuki Fujisawa, and Makoto Yamashita. The second-order reduced density matrix method and the two-dimensional hubbard model. *Comp. Theo. Chem.*, 1003(0):22 – 27, 2013.

[3] P. W. Anderson. The resonating valence bond state in La2CuO4 and superconductivity. *Science*, 235(4793):1196–1198, March 1987.

[4] Philip W Anderson. Superconductivity in high tc cuprates: The cause is no longer a mystery. *Physica Scripta*, pages 10–12.

[5] John Bardeen, Leon N Cooper, and J Robert Schrieffer. Theory of superconductivity. *Physical Review*, 108(5):1175, 1957.

[6] J. G. Bednorz and K. A. Müller. Possible high tc superconductivity in the ba-la-cu-o system. *Zeitschrift für Physik B Condensed Matter*, 64(2):189–193, 1986.

[7] R.J. Cava, T. Siegrist, B. Hessen, J.J. Krajewski, W.F. Peck Jr., B. Batlogg, H. Takagi, J.V. Waszczak, L.F. Schneemeyer, and H.W. Zandbergen. A new homologous series of lanthanum copper oxides. *J. Solid State Chem.*, 94(1):170 – 184, 1991.

[8] Yao-Hua Chen, Hong-Shuai Tao, Dao-Xin Yao, and Wu-Ming Liu. Kondo metal and ferrimagnetic insulator on the triangular kagome lattice. *Phys. Rev. Lett.*, 108:246402, Jun 2012.

[9] Yao-Hua Chen, Wei Wu, Hong-Shuai Tao, and Wu-Ming Liu. Cold atoms in a two-

dimensional triangular optical lattice as an artificial frustrated system. *Phys. Rev. A*, 82:043625, Oct 2010.

[10] A. J. Coleman and I. Absar. *Int. J. Quant. Chem.*, 18:1279, 1980.

[11] Elbio Dagotto. Correlated electrons in high-temperature superconductors. *Rev. Mod. Phys.*, 66:763–840, Jul 1994.

[12] Elbio Dagotto and T. M. Rice. Surprises on the way from one- to two-dimensional quantum magnets: The ladder materials. *Science*, 271(5249):618–623, February 1996.

[13] Fabian H. L. Essler, Vladimir E. Korepin, and Kareljan Schoutens. Complete solution of the one-dimensional hubbard model. *Phys. Rev. Lett.*, 67:3848–3851, Dec 1991.

[14] M. Fabrizio, A. Parola, and E. Tosatti. Strong-coupling phases of two hubbard chains with interchain hopping. *Phys. Rev. B*, 46:3159–3162, Aug 1992.

[15] L Gao, YY Xue, F Chen, Q Xiong, RL Meng, D Ramirez, CW Chu, JH Eggert, and HK Mao. Superconductivity up to 164 k in hgba 2 ca m- 1 cu m o 2 m+ 2+ δ (m= 1, 2, and 3) under quasihydrostatic pressures. *Physical Review B*, 50(6):4260, 1994.

[16] Gergely Gidofalvi and David A. Mazziotti. Spin and symmetry adaptation of the variational two-electron reduced-density-matrix method. *Phys. Rev. A*, 72:052505, Nov 2005.

[17] Martin C. Gutzwiller. Effect of correlation on the ferromagnetism of transition metals. *Phys. Rev. Lett.*, 10:159–162, Mar 1963.

[18] Martin C. Gutzwiller. Correlation of electrons in a narrow s band. *Phys. Rev.*, 137:A1726–A1735, Mar 1965.

[19] Jeff R. Hammond and David A. Mazziotti. Variational two-electron reduced-density-matrix theory: Partial 3-positivity conditions for n-representability. *Phys. Rev. A*, 71(6):062503, June 2005.

[20] Z. Hiroi, M. Azuma, M. Takano, and Y. Bando. A new homologous series srn1cun+1o2n found in the srocuo system treated under high pressure. *J. Solid State Chem.*, 95(1):230 – 238, 1991.

[21] J. Hubbard. Electron correlations in narrow energy bands. *Proc. R. Soc. Lond. A*, 276(1365):238–257, November 1963.

[22] T. Juhász and David A. Mazziotti. The cumulant two-particle reduced density matrix as a measure of electron correlation and entanglement. *J. Chem. Phys.*, 125(17):–, 2006.

[23] C. P. Landee, M. M. Turnbull, C. Galeriu, J. Giantsidis, and F. M. Woodward. Magnetic properties of a molecular-based spin-ladder system. *Phys. Rev. B*, 63:100402, Feb 2001.

[24] Anthony J Leggett. What do we know about high tc? *Nature Physics*, 2(3):134–136, 2006.

[25] D. A. Mazziotti. 3,5-contracted schrödinger equation: Determining quantum energies and reduced density matrices without wave functions. *Int. J. Quantum Chem.*, 70:557, 1998.

[26] D. A. Mazziotti. Approximate solution for electron correlation through the use of schwinger probes. *Chem. Phys. Lett.*, 289:419, 1998.

[27] D. A. Mazziotti. Contracted schrodinger equation: Determining quantum energies and two-particle density matrices without wave functions. *Phys. Rev. A*, 57:4219–4234, 1998.

[28] David A. Mazziotti. Variational two-electron reduced density matrix theory for many-electron atoms and molecules: Implementation of the spin- and symmetry-adapted T_2

condition through first-order semidefinite programming. *Phys. Rev. A*, 72:032510, Sep 2005.

[29] R.M. Noack, S.R. White, and D.J. Scalapino. The ground state of the two-leg hubbard ladder a density-matrix renormalization group study. *Physica C*, 270(34):281 – 296, 1996.

[30] R. Norrestam, M. Nygren, and J.-O. Bovin. New intermediate phases of the composition la2n+2cun+4o4n+7 in the la-cu-o system: The crystal structure and thermal stability of la2cu2o5. *Angew. Chem. Int. Ed.*, 30(7):864–866, 1991.

[31] Takuma Ohashi, Norio Kawakami, and Hirokazu Tsunetsugu. Mott transition in kagom lattice hubbard model. *Phys. Rev. Lett.*, 97:066401, Aug 2006.

[32] F. R. Petruziel, A. A. Holmes, Hitesh J. Changlani, M. P. Nightingale, and C. J. Umrigar. *Phys. Rev. Lett.*, 109:230201, 2012.

[33] R. R. Rodriguez-Guzman, C. A. Jimenez-Hoyos, R. Schutski, and G. E. Scuseria. Multireference symmetry-projected variational approaches for ground and excited states of the one-dimensional hubbard model. *Phys. Rev. B*, 87:235129, 2013.

[34] W. Slebodzinski. *Exterior Forms and Their Application.* Polish Scientific Publishers, Warsaw, 1970.

[35] Brecht Verstichel, Ward Poelmans, Stijn De Baerdemacker, Sebastian Wouters, and Dimitri Van Neck. Variational optimization of the 2dm: approaching three-index accuracy using extended cluster constraints. *The European Physical Journal B*, 87(3):1–11, 2014.

[36] Brecht Verstichel, Helen van Aggelen, Ward Poelmans, and Dimitri Van Neck. Variational two-particle density matrix calculation for the hubbard model below half filling using spin-adapted lifting conditions. *Phys. Rev. Lett.*, 108(21):213001, may 2012.

[37] Brecht Verstichel, Helen van Aggelen, Ward Poelmans, Sebastian Wouters, and Dimitri Van Neck. Extensive v2dm study of the one-dimensional hubbard model for large lattice sizes: Exploiting translational invariance and parity. *Comp. Theo. Chem.*, 1003(0):12 – 21, 2013.

[38] M. K. Wu, J. R. Ashburn, C. J. Torng, P. H. Hor, R. L. Meng, L. Gao, Z. J. Huang, Y. Q. Wang, and C. W. Chu. Superconductivity at 93 k in a new mixed-phase y-ba-cu-o compound system at ambient pressure. *Phys. Rev. Lett.*, 58:908–910, Mar 1987.

[39] Wei Wu, Yao-Hua Chen, Hong-Shuai Tao, Ning-Hua Tong, and Wu-Ming Liu. Interacting dirac fermions on honeycomb lattice. *Phys. Rev. B*, 82:245102, Dec 2010.

CHAPTER 4

STRONG ELECTRON CORRELATION IN MATERIALS FROM PAIR-INTERACTING MODEL HAMILTONIANS

This chapter contains parts of the published work [N. C. Rubin, and D. A. Mazziotti, *J. Phys. Chem. C* 119 (26), 1470614713, (**2015**)]

4.1 Overview

Model Hamiltonians that can emulate key features of solid-state materials offer an opportunity to study electronic systems at different degrees of strong electron correlation, which is important for elucidating a range of phenomena including high-temperature superconductivity and quantum phase transitions. There is a plethora of model spin Hamiltonians including the Heisenberg, Hubbard, and t-J Hamiltonians that build in pairing [29, 20, 9], on-site interaction [19], or nearest-neighbor interactions [21] that induce strong correlations. Many of these models focus on the competition between localization and delocalization from kinetic and potential energy terms in the Hamiltonian as a generator for electron correlation [23]. It is typically found that this type of model can be described by a mean-field wave function in a particular limit that provides a reasonable reference in a perturbation-theory framework for a more correlated description.

We examine different degrees of strong electron correlation found in materials through a class of model pairing Hamiltonians. We focus on the pairing Hamiltonians, previously defined by Erdahl and Jin, that lack any one-electron term [22, 11]. The potential in the Hamiltonian defines an interaction between pairs of electrons, and the kinetic energy in the Hamilton defines the transport of pairs of electrons. For the range of parameters in the model Hamiltonians the ground-state wave functions possess a common one electron-reduced density matrix (1-RDM). Because the two-electron interactions are not universal

to all of the Hamiltonians in the model, the Hohenberg-Kohn theorem [18] does not apply, and one-electron theories like Hartree-Fock and density functional theory are largely either inaccurate or inapplicable.

In one limit of the Hamiltonian's parameters the ground states are superconducting states describable by projected Bardeen-Cooper-Schrieffer (BCS) wave functions [3, 32], also known as antisymmetrized geminal power (AGP) wave functions [6, 7, 8, 25, 16], and in another limit the ground states are locally ordered states in which the kinetic energy is quenched. Between these two limits model Hamiltonian express more general family of pairing wave functions that describe long-range order and pairing phenomena beyond superconductivity that is potentially important for molecules and materials with novel properties arising from strong electron correlation.

In a system with only pair interactions the *two-electron reduced density matrix* (2-RDM) is a natural descriptor. By Rosina's theorem there exists a one-to-one mapping between each ground-state 2-RDM and each energetically non-degenerate ground-state wave function [24]. Importantly, the 2-RDM-to-wave-function map in Rosina's theorem only requires that the interaction terms be two-body. In contrast, the mapping between the ground-state 1-RDM (or 1-electron density) and the wave function in the Hohenberg-Kohn theorem [18] requires specific knowledge of the Hamiltonian's interaction terms to make the mapping one-to-one [24]. Originally shown by Yang [41], the 2-RDM is the most compact representation of a fermionic N-particle system with superconducting character. As such the 2-RDM has been extensively utilized in the study of pair-correlation dominated Hamiltonians like model superconductors [41, 31, 15, 4, 36, 30] and repulsive Hubbard models in the high U limit [33, 39, 38, 1, 17].

After developing the class of model pairing Hamiltonians, we variationally compute the 2-RDM for a range of lattices including linear, ladder, and square topologies. We also investigate the possible superconducting gap parameter based on the three lattice topologies.

We find that for all model Hamiltonians the 2-RDM is accurately computed as long as the D, Q, and G N-representability conditions [8, 5, 12], also known as the (2,2)-positivity conditions, are supplemented with the T2 condition [10, 42, 26], a member of the (2,3)-positivity conditions [27]. Energies, orbital and geminal occupation numbers, and correlation functions are computed. As shown by Yang [41] as well as Sasaki [5, 34], the largest geminal occupation number of the 2-RDM reveals long-range order when it is on the order of the number N of electrons. The model has applications to superconductivity as well as more general pairing phenomena in electronic systems while the variational calculation of the 2-RDM has applications to studying electronic structure in a wide range of strongly correlated quantum systems.

4.2 Theory

4.2.1 Model System

The Hamiltonian was derived from the set of generators forming a SU(2) Lie algebra and contains only two-body interactions [22]. The superconducting model is defined on one-, two-, or three-dimensional cubic lattice with equally spaced sites ($\{\Lambda\}$). General properties of the Hamiltonian such as its action on states built from pair operators, ground state properties for small linear lattices, and the existence of alternating and constant phase antisymmeterized geminal power (AGP) ground states has been previously reported [11, 22]. When expressed in normal ordering the Hamiltonian is composed of two pieces; a nearest-neighbor Coulomb

component $\hat{H}_e$ and nearest-neighbor pair transport $\hat{H}_t$

$$\begin{aligned}\hat{H}_e =&\alpha_e \left[C_\rho + \sum_i \sum_\sigma \left(\hat{a}^\dagger_{i+1\sigma} \hat{a}^\dagger_{i\sigma} \hat{a}_{i\sigma} \hat{a}_{i+1\sigma} \right.\right. \\ &\left.\left. + \hat{a}^\dagger_{i+1\sigma} \hat{a}^\dagger_{i-\sigma} \hat{a}_{i-\sigma} \hat{a}_{i+1\sigma} \right) \right] \end{aligned} \tag{4.1}$$

$$\begin{aligned}\hat{H}_t =&\alpha_t \sum_i \left(\hat{a}^\dagger_{i+1\alpha} \hat{a}^\dagger_{i+1\beta} \hat{a}_{i\beta} \hat{a}_{i\alpha} + \hat{a}^\dagger_{i\alpha} \hat{a}^\dagger_{i\beta} \hat{a}_{i+1\beta} \hat{a}_{i+1\alpha} \right) \\ \hat{H} =&\hat{H}_t + \hat{H}_e \end{aligned} \tag{4.2}$$

where $\hat{a}^\dagger_{j\sigma}$ ($\hat{a}_{j\sigma}$) creates (annihilates) a fermion at site j with spin σ, α_e and α_t are the electrostatic and transport strengths, and C_ρ is number of nearest neighbor pairs minus the twice the total density of electrons. The constant term comes from expressing the pure two-body Hamiltonian in normal ordering using the fermionic anticommutation relations. This term only depends on diagonal elements of the 1-RDM and simply shifts the energy levels.

The Hamiltonian projects a pairing subspace formed from

$$\eta^\dagger_i = \hat{a}^\dagger_{i\alpha} \hat{a}^\dagger_{i\beta} \tag{4.3}$$

operators that create a spin-zero particle on each site. The total wave function is constructed from the N_a choose M determinants of η where N_a is the total number of orbitals and M is the number of pairs on the lattice. The 1-RDMs from these wave functions are diagonal because η operator creates pairs of electrons on the lattices and thus single-particle correlations corresponding to off-diagonal elements in the 1-RDM are zero. Calculations are performed at half filling, and thus, each diagonal elements of the α spin block of the 1-RDM is equal to one-half. This special structure is independent of the Hamiltonian parameters.

4.3 Results

In section 4.3 we present the results from applying the variational 2-RDM method with the D, Q, G, and T2 conditions to the pair-interaction model Hamiltonians. We present the convex set of 2-RDMs generated by the class of model Hamiltonians under complete and incomplete N-representability conditions in section 4.3.1. Energies, orbital and geminal occupation numbers, and correlation functions are reported in the remaining sections.

4.3.1 N-representable Region

The N-representable region is quantified by the expectation value of any hermitian operator against ${}^2D$ to be positive semidefinite. By taking the expectation of the unscaled Hamiltonian operators, Coulomb and transport, we trace out a useful projection of the total representable region. This method of projection down from the full representable region has been previously used as a phase diagram to analyze transition in the Ising and Lipkin models [14, 35]. Here we use it to asses the accuracy captured by approximate N-representability for each component of the Hamiltonian. For our Hamiltonian, parametrized by the vector α defined in Eq. (4.4), we define expectation values β as the projection of the Coulomb and the pair transport part of the Hamiltonian, Eq. (4.5), on the ground state 2-RDM.

$$\alpha = (\alpha_e, \alpha_t) \tag{4.4}$$

$$\beta = \left(\mathrm{Tr}\left[{}^2H_e \, {}^2D \right], \mathrm{Tr}\left[{}^2H_t \, {}^2D \right] \right) \tag{4.5}$$

where ${}^2H_e$ and ${}^2H_t$ correspond to the reduced Hamiltonians of the nearest-neighbor Coulomb and nearest-neighbor transport parts of the total Hamiltonian. The set of points $\{\beta\}$ are the extreme points of the representable set. This set is determined numerically by finding

the ground state 2-RDM at Hamiltonian parameters α in the following regions:

$$[\alpha_e, \alpha_t] = [\theta, -1]\,, \quad -1 \leq \theta \leq 1 \tag{4.6}$$

$$= [1, \theta]\,, \quad -1 \leq \theta \leq 0 \tag{4.7}$$

$$= [1, \theta]\,, \quad 0 \leq \theta \leq 1 \tag{4.8}$$

$$= [-\theta, 1]\,, \quad -1 \leq \theta \leq 1 \tag{4.9}$$

In Fig. 4.1 we have plotted the representable region for the 1×16 lattice with periodic boundary conditions computed with the variational 2-RDM methodology using two sets of N-representability constraints. We compare the approximate 2-RDMs with 2-RDMs contracted from an exact diagonalization calculation. The curves in Fig. 4.1 correspond to the representable boundary. Points on the interior correspond with excited state 2-RDMs. The region is symmetric around the axis $\beta_t = 0$ and therefore we only plot the region defined by α of Eqs (4.6, 4.7). The straight line from point $(0, 1)$ to point labeled (A) are AGP states with even particle numbers. All superconducting constant phase AGP wave functions are located along this line. We find, as previously reported [11, 22], that DQG fails to capture the boundary of the region away from the AGP states.

4.3.2 Energy Results

In Table 4.1 we have compiled the ground state energy given two Hamiltonian parameters calculated with DQG and DQGT constraints on a linear lattice with periodic boundary conditions. Each ground state corresponds to a point along the boundary of the representable region. The superconducting states $(\alpha_t, \alpha_e) = (-1, -1)$ starting from zero particles to half filling all have zero energy as the dimension dependent constant counting the number of nearest-neighbors has been dropped. In this region DQG and DQGT capture the ground state energy exactly. Any deviation away from 100 percent correlation captured corresponds

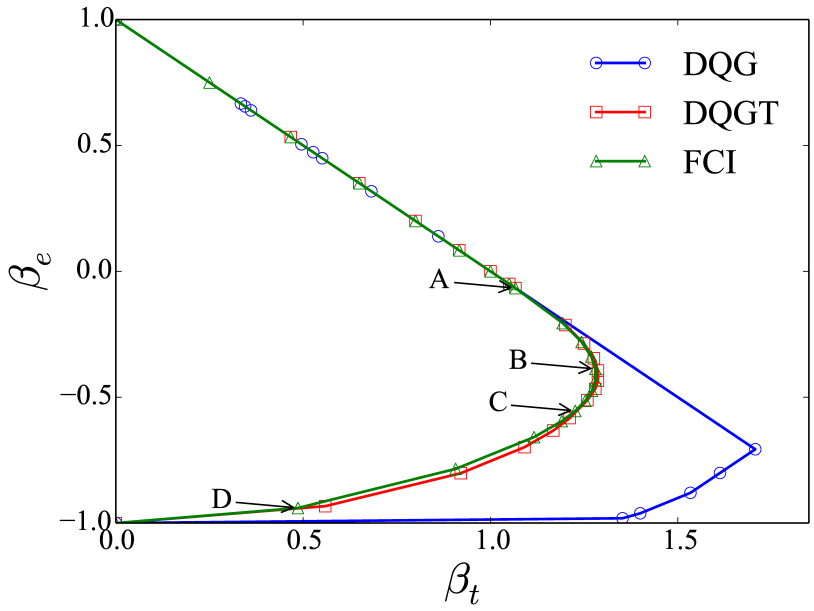

Figure 4.1: N-representable region for the 1×16 lattice calculated with exact diagonalization, DQG, and DQGT conditions. The region is symmetric around $\beta_t = 0$. The labeled points correspond to (α_t, α_e) $A = (-1.0000, -1.0000)$, $B = (-1.0000, -0.1111)$, $C = (1.0000, 0.7778)$, $D = (-0.2500, 1.0000)$

to numerical errors which in test cases were eliminated with tighter SDP convergence criteria. The (2,2)-positivity, DQG, conditions produce energies significantly below the exact diagonalization energy. The largest error of 10.05 a.u. occurs when the difference between the nearest-neighbor repulsion and pair transport are maximal at $\alpha = (1, -1)$. DQGT accurately reproduce the ground state energy over the entire representable region. The largest error from exact diagonalization for the ground state energy calculated with DQGT was 0.384 a.u. and occurred when $\alpha = (1, -0.5)$.

The percent correlation captured is calculated relative to a single closed shell determinant found to be the lowest energy in the manifold of restricted closed shell determinants. To determine the lowest energy determinant, all states on Fock space are evaluated against the exact reduced Hamiltonian by the following expression

$$E_{MF} = \mathrm{Tr}\left[{}^2K\ ({}^1D_{\mathrm{MF}} \wedge {}^1D_{\mathrm{MF}})\right] \tag{4.10}$$

where ${}^1D_{\mathrm{MF}}$ is the 1-RDM generated from the closed shell reference state. This methodology produces a class of degenerate functions which can be mapped onto one another by the translational operators supported by the lattice. Though the exact 1-RDM of the system is invariant to Hamiltonian parameters a closed shell determinant reference is selected because it is closest to an uncorrelated description of the system. It was found that the best reference switched from all particles grouped together for $\alpha_e < 0$ to checkerboard states with $\alpha_e > 0$. This simply reflects what interaction types are penalized with the change in sign of the nearest-neighbor Coulomb interaction.

The maximal correlation energy captured reflects the location of the largest errors with respect to energy. In Fig. 4.2 we have plotted the correlation energy captured by DQGT (DQG is inset) on a linear, ladder and square lattice of sixteen orbitals at half filling. The straight line with zero error for both DQG and DQGT on boundary points (points numbered $[0, 8]$) correspond to a constant phase AGP state ground state. Once beyond those points along the boundary, the DQG solution significantly deviates from the exact diagonalize energy. The area with the largest error corresponds to the region of farthest from the FCI representable region if Fig. 4.1.

4.3.3 Symmetry of the ground-state wave function

Symmetry of the AGP wave function has been shown the be synonymous with the symmetry of the superconducting gap function Δ[2, 37]. We directly symmetry adapt the ground state 2-RDM for the linear, ladder and square lattices with C_i, C_{2v}, and C_{4v} respectively. The 2-RDM is a blocked matrix in any point group symmetry by the following expression

$$ {}^2D^{i'\Gamma_i j'\Gamma_j}_{k'\Gamma_k l'\Gamma_l} = \langle\psi|\hat{a}^\dagger_{i'\Gamma_i}\hat{a}^\dagger_{j'\Gamma_j}\hat{a}_{l'\Gamma_l}\hat{a}_{k'\Gamma_k}|\psi\rangle \tag{4.11} $$

Table 4.1: Ground state energies (in dimensionless units) of a 1×16 lattice computed with the mean-field reference, variational RDM with DQG and DQGT N-representability constraints, and exact diagonalization (FCI). α_e and α_t correspond to the strength of nearest-neighbor Coulomb interaction and nearest-neighbor pair transport, respectively.

Label	α_e	α_t	$E_{\mathrm{M-F}}$	E_{DQG}	E_{DQGT}	E_{FCI}
1	−1.0000	−1.0000	0.0000	0.0000	0.0000	0.0000
2	−1.0000	−1.0000	0.0000	0.0000	0.0000	0.0000
3	−1.0000	−1.0000	0.8333	0.0000	0.0000	0.0000
4	−1.0000	−1.0000	1.0000	0.0000	0.0000	0.0000
5	−1.0000	−1.0000	1.0714	0.0000	0.0000	0.0000
6	−1.0000	−1.0000	1.1111	0.0000	0.0000	0.0000
7	−1.0000	−1.0000	1.1364	0.0000	0.0000	0.0000
8	−1.0000	−1.0000	1.1538	0.0000	0.0000	0.0000
9	−1.0000	−1.0000	1.1667	0.0000	0.0000	0.0000
10	−0.7778	−1.0000	0.9074	−6.0688	−4.1016	−4.0819
11	−0.5556	−1.0000	0.6481	−12.1378	−8.5563	−8.5093
12	−0.3333	−1.0000	0.3889	−18.2067	−13.2389	−13.1680
13	−0.1111	−1.0000	0.1296	−24.2756	−18.1126	−18.0158
14	0.1111	−1.0000	−2.0741	−30.3444	−23.1429	−23.0305
15	0.3333	−1.0000	−6.2222	−36.4133	−28.3013	−28.1988
16	0.5556	−1.0000	−10.3704	−42.4822	−33.5777	−33.5130
17	0.7778	−1.0000	−14.5185	−48.5511	−39.0855	−38.9697
18	1.0000	−1.0000	−18.6667	−54.6200	−44.8036	−44.5692
19	1.0000	−0.7500	−18.6667	−48.4844	−40.2671	−39.9333
20	1.0000	−0.5000	−18.6667	−42.5794	−36.1972	−35.8132
21	1.0000	−0.2500	−18.6667	−37.1055	−33.1607	−32.9854
22	1.0000	0.0000	−18.6667	−32.0000	−32.0000	−32.0000

where $\Gamma_i \otimes \Gamma_j$ and $\Gamma_l \otimes \Gamma_k$ must contain the totally symmetric representation [13]. Direct products of irreducible representations in Abelian groups decompose into a single irreducible representation while this guarantee is not maintained for irreducible representations of non-Abelian groups such as C_{4v}. In the C_{4v} case the $E \otimes E$ group connects to all other blocks of the 2-RDM destroying the block-diagonal structure.

We have found that for the linear and ladder cases the superconducting state is of A_1 symmetry (s-wave) for both the constant and alternating phase ground state AGP wave functions. Analysis of the natural 2-state reveals the pairing wave functions are formed with on-site pairs. Symmetry adapting the 2-RDM of the square lattices under the lattice

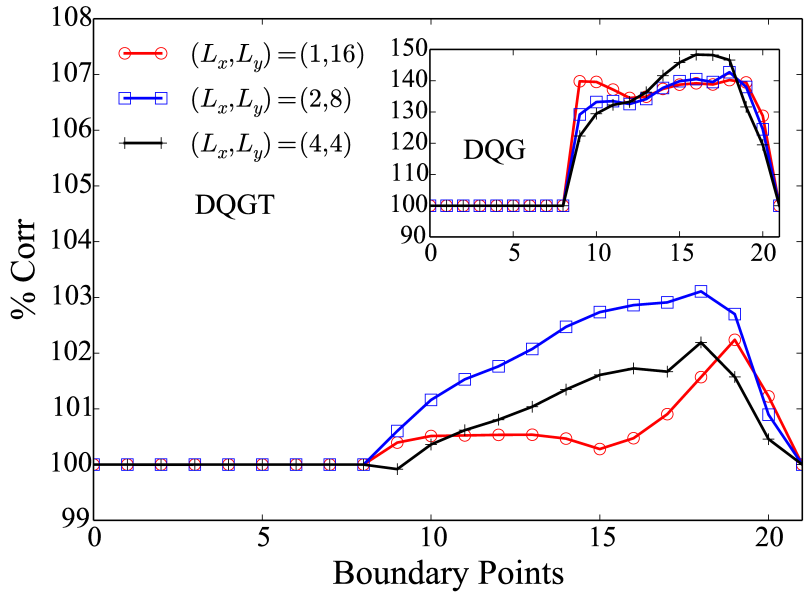

Figure 4.2: Percent of the correlation energy recovered with DQGT conditions (inset are results from DQG conditions) on a 1×16, 2×8, and 4×4 lattice. Boundary points correspond with labels for (α_e, α_t) points in Table 4.1.

symmetry C_{4v}, we find that the alternating phase and constant phase AGP wave functions correspond to d_{xy}-wave (space irreducible representation B_2) and s-wave (space irreducible representation A_1) symmetry respectively [40]. Analysis of the natural 2-state reveals the pairing wave functions are formed with on-site pairs. Bond-singlet formation necessary for $d_{x^2-y^2}$-wave superconductivity is therefore most likely difficult to achieve in this model augmented with other Hamiltonians that form the set specified by the nearest-neighbor set [22].

4.3.4 Natural Orbital Occupation Numbers

The variational RDM method has no knowledge of the Hamiltonian's ability to project out wave functions built from the η operator. Therefore, the ability to capture the diagonal nature of the 1-RDM and largest eigenvalue of the 2-RDM is an important accuracy check for approximate N-representability. In Table 4.2 we have tabulated the maximum 2-RDM

eigenvalue at four points (labeled in Fig. 4.1) along the boundary of the representable region. The 1-RDM is diagonal with elements reflecting the density of the system. At half filling

Table 4.2: The maximum 2-RDM eigenvalue for linear, ladder, and square lattices of sixteen orbitals at half filling calculated with DQG, DQGT, and exact diagonalization (FCI).

		${}^2\lambda_{\max}$		
Lattice	(α_t, α_e)	DQG	DQGT	FCI
1×16	A	0.839364	4.500000	4.500000
	B	1.781339	3.178220	3.298490
	C	1.784177	2.503490	2.357758
	D	1.499989	0.989341	0.790922
2×8	A	1.395260	4.500000	4.500000
	B	2.452881	3.758220	3.968119
	C	2.399076	2.663333	2.798911
	D	1.000003	0.766539	0.718440
4×4	A	1.920349	4.500000	4.500000
	B	4.000000	4.238733	4.299764
	C	4.000000	3.499314	3.540278
	D	1.000000	0.722291	0.693338

each diagonal element of the exact 1-RDM is 0.5. This value is faithfully captured by both DQG and DQGT for all interaction strengths. The largest eigenvalue of the 2-RDM at the superconducting state is reproduced exactly by DQGT. At all other points along the boundary the maximum eigenvalues of the 2-RDM from DQGT calculations closely follow the eigenvalues from exact diagonalization. Despite an accurate ground state energy at the superconducting points, DQG gives the wrong large eigenvalues reflecting the incorrect structure of the 2-RDM. In order to further examine the accuracy of 2-RDM elements with both sets of N-representability conditions we examine correlation functions defined from diagonal elements (classical correlators) and off diagonal elements (quantum correlators).

4.3.5 Correlation functions

We analyze the structure of off-diagonal elements using the η-pairing correlation function and a classical correlation function to describe charge-ordering on the lattice at four points along the boundary of the representable region.

Classical Correlation: Pairing Separation

Classical correlators correspond to averages over diagonal elements of density matrices. In this class are spin and charge correlation functions commonly used to study lattice models [33, 39]. To examine charge ordering, we utilize the standard charge correlation function

$$\langle \hat{n}_i \hat{n}_{i+R} \rangle \tag{4.12}$$

where

$$\hat{n}_i = \hat{a}^\dagger_{i\alpha} \hat{a}_{i\alpha} + \hat{a}^\dagger_{i\beta} \hat{a}_{i\beta} \tag{4.13}$$

and express it as a function of the 2-RDM.

$$\begin{aligned} \langle \hat{n}_i \hat{n}_{i+R} \rangle = &\left(\hat{a}^\dagger_{i\alpha} \hat{a}_{i\alpha} + \hat{a}^\dagger_{i\beta} \hat{a}_{i\beta} \right) \times \\ &\left(\hat{a}^\dagger_{i+R\alpha} \hat{a}_{i+R\alpha} + \hat{a}^\dagger_{i+R\beta} \hat{a}_{i+R\beta} \right) && (4.14) \\ = &\sum_\sigma \hat{a}^\dagger_{i\sigma} \hat{a}^\dagger_{i+R\sigma} \hat{a}_{i+R\sigma} \hat{a}_{i\sigma} + && (4.15) \\ &\sum_\sigma \hat{a}^\dagger_{i,\sigma} \hat{a}^\dagger_{i+R,-\sigma} \hat{a}_{i+R,-\sigma} \hat{a}_{i,\sigma} && (4.16) \end{aligned}$$

The correlation function is divided into expectations over the symmetric and antisymmetric pieces of the 2-RDM.

In Fig. 4.3 we have plotted the charge correlation defined in Eq. (4.12) at three points along the boundary. At the superconducting state we have equal likelihood of pair occupation

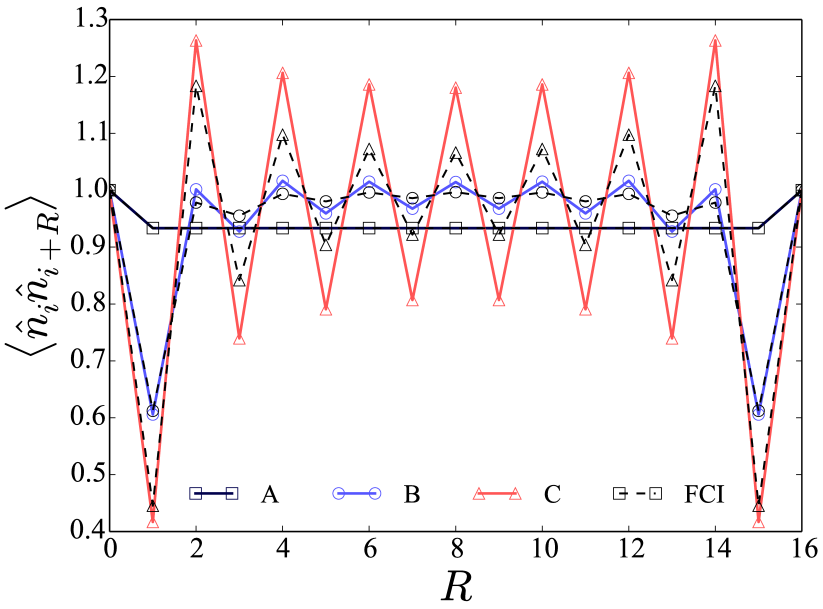

Figure 4.3: Charge correlation on the 1×16 lattice calculated with DQGT (solid line) and FCI (dashed lines). Point D is left off the graph as the checkerboard state results in a correlation function that dominates the magnitude of the graph making other states indistinguishable.

across the lattice. As pairs are localized at point B on the representable region a nearest-neighbor pair-hole develops and we see a decay similar to the Heisenberg antiferromagnet spin correlation function. Finally, at the point of maximal classical correlation we have a superposition of two ground state determinants corresponding to two checkerboard states. This point on the boundary is referred to as classical because there are no off-diagonal elements in the 2-RDM connecting the two states. DQGT captures all the structure in the correlation function but over estimates the relative amplitudes of diagonal 2-RDM elements. This corresponds to DQGT over localizing pairs. It has been previously shown in Ref. [[22]] that under a partial particle hole transformation the Hamiltonian is isomorphic with the Heisenberg spin model. Thus, we expect that the pair-charge correlations away from the AGP state are similar to the antiferromagnet correlation functions in one-, quasi-one, and two-dimensions.

η-pairing for lattices

The η-pairing correlation function gives the expectation value for pair transmission between two sites on the lattice. At the superconducting state in the thermodynamic limit all sites have equal probability of transport with each other yielding a large eigenvalue of the 2-RDM. We plot the η-pairing correlation function for a linear, ladder, and square lattice of sixteen spatial orbitals each to assess the accuracy of N-representability enforced through DQGT conditions. The η-pairing correlation function

$$\langle \hat{\eta}_i^\dagger \hat{\eta}_j \rangle = \langle \hat{a}_{i\alpha}^\dagger \hat{a}_{i\beta}^\dagger \hat{a}_{j\beta} \hat{a}_{j\alpha} \rangle \tag{4.17}$$

where i and j can take on any distance supported by the lattice, corresponds non-zero elements in the connected piece of the 2-RDM thus capturing information completely beyond a one-particle model of the electronic structure. Figure 4.4 is the η-pairing correlation function for the 1×16 lattice at four selected points along the boundary calculated from a DQGT 2-RDM and an exact diagonalization 2-RDM. Point A is the superconducting state at half filling. The flat line across indicates the hopping amplitude of pairs of electrons is equal and thus leading to a maximal eigenvalue in the 2-RDM. The values are not equal to the thermodynamic limit because of finite size effects. As the lattice increases in size the off diagonal elements approach the thermodynamic value. The correlation function is symmetric around the inversion center of the lattice due to the periodic boundary conditions.

Analysis of FCI results suggest that as we traverse the boundary from the superconducting point to the checker board state electron pairs localize in a continuous fashion. We can observe the loss of off-diagonal long-range order (ODLRO) and localization by directly using the largest eigenvalue of the 2-RDM as an order parameter. In Figure 4.5 the largest eigenvalue of the 2-RDM is plotted as we traverse the boundary of the representable region. $\lambda_{\max}$ matches the bound given by Yang and Coleman [7, 41] at the superconducting points and

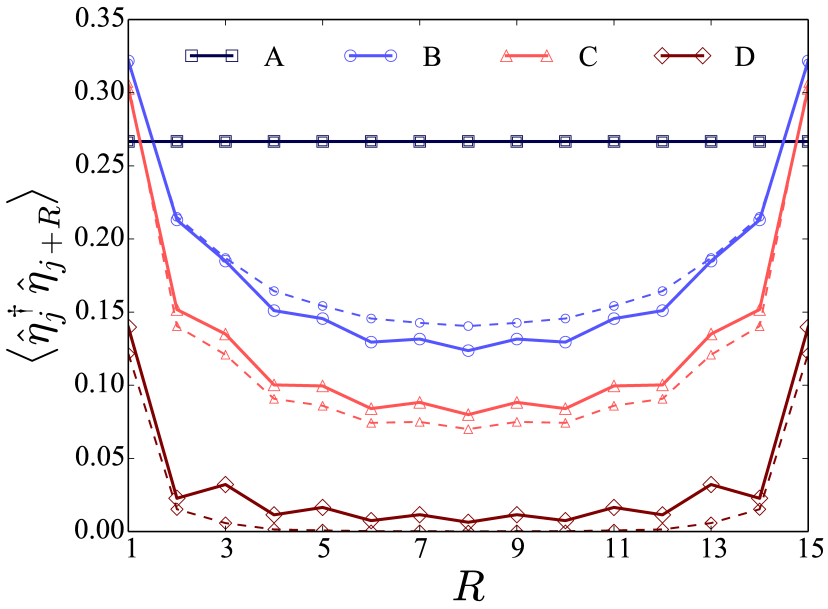

Figure 4.4: Expectation value of $\langle \eta_j^\dagger \eta_{j+R} \rangle$ from calculation with DQGT constraints (solid line). Dashed line is correlation function calculated from FCI 2-RDM

decays away to after the AGP is broken to a variational η-pair wave function. Furthermore, significant finite size effects are observed in the curvature of $\lambda_{\max}$ between points A and D.

Similarly In Fig. 4.6 we have plotted the ODLRO correlation function for the 2×8 and 4×4 lattice. The four charts on each line of Fig. 4.6 correspond to the four ground state 2-RDMs labeled in Fig. 4.1. The large value at $(x, y) = (1, 1)$ in all the charts is the diagonal element of the 2-RDM which reflects the particle density on the lattice and is constant for all 2-RDMs with fixed trace. Each bar corresponds to the value of the η-pair correlation function on a real-space lattice. Despite significant finite size effects in the 4×4 case we can still directly observe the loss of ODLRO and emergence of classical correlations. At the superconducting state pairs have equal transmission probability between all sites on the lattice. In the ladder and square cases we observe pairs being localized at similar rates.

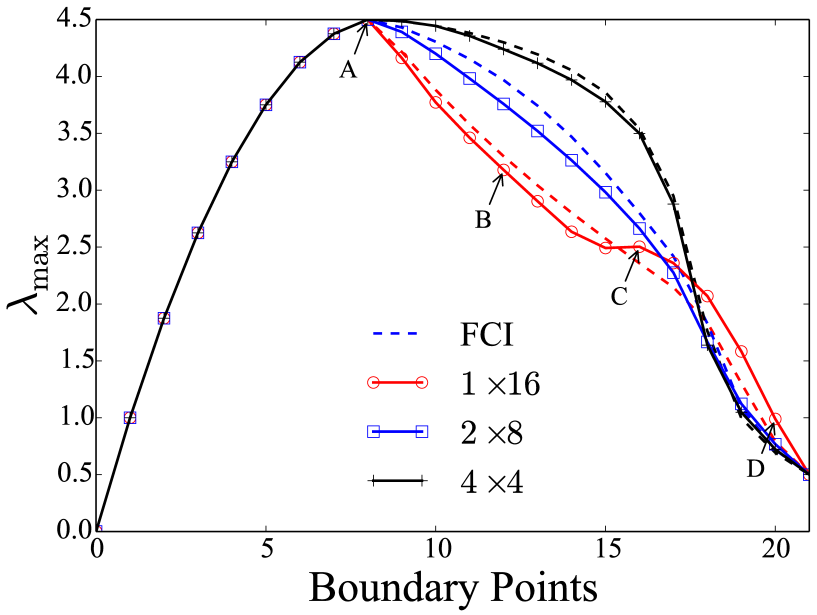

Figure 4.5: Largest eigenvalue of the 2-RDM ($\lambda_{\max}$) for a 1×16, 2×8, and 4×4 lattices. FCI is plotted in dashed lines with the corresponding color.

4.4 Discussion and Conclusions

A class of pair-interacting model Hamiltonians has been explored computationally for the description of different levels of strong electron correlation in materials. Because the Hamiltonians contain only terms with electron interactions, their ground-state wave functions are indescribable by a single Slater determinant. More importantly, each model Hamiltonian shares the same diagonal 1-RDM in the site basis set with uniform occupations. Since the 1-RDM including its natural orbitals and occupations lacks any dependence on the Hamiltonian's parameters, one-electron models of the correlation such as the Hartree-Fock method and density functional theory are either inaccurate or inapplicable. In contrast to the 1-RDM, there exists a one-to-one mapping between the ground-state 2-RDM and the ground-state wave function for each model Hamiltonian as long as the ground state is energetically non-degenerate [24].

For linear, ladder, and square topologies we variationally computed the ground-state 2-RDMs of the model Hamiltonians across a full range of parameters. Energies, correla-

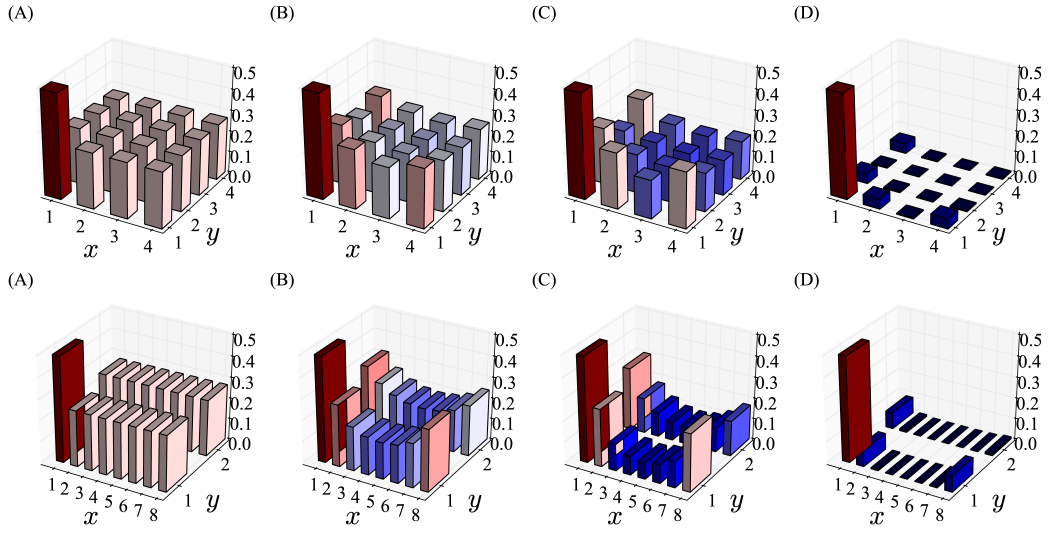

Figure 4.6: top) 4×4 and bottom) 2×8 η-pairing expectations as we deviate away from the AGP state. x-y-axis indicates position on the direct lattice while the z-axis is the expectation value given in Eq. (4.17)

tion functions, as well as orbital and geminal occupation numbers were computed. In the variational calculations the 2-RDM was constrained by a subset of the N-representability conditions that are necessary for it to represent an ensemble N-electron system. We found that using the D, Q, G, and T2 N-representability conditions [10, 42, 26] generated accurate energies and observables for the full-spectrum of model Hamiltonians. The T2 condition was observed to be particularly important to capturing strong electron correlation accurately for general pairing phenomena that is not describable by traditional BCS or AGP wave functions [3, 32, 6, 7, 8, 25, 16]. Furthermore, the T2 condition reproduced the accuracy observed in previous calculations by Erdahl and Jin [22, 11], which employed the more expensive positivity conditions on the 3-RDM [28].

In one limit the model Hamiltonians yield superconducting ground states that are exactly describable by projected BCS (AGP) wave functions, and in another limit they yield locally ordered ground states. Between these two limits the Hamiltonians produce a pairing phenomenon that is more general than that found in superconductivity. The largest eigenvalue of the 2-RDM reveals long-range order in both the superconducting and general pairing regimes.

These more general pairing states are likely important in understanding how strong electron correlation influences the behavior of novel molecules and materials. The model Hamiltonians in conjunction with the direct variational 2-RDM calculations provide a framework for exploring strong electron correlation in molecules and materials, particularly in the regime where one-electron theories or perturbation-based methods are inaccurate.

4.5 References

[1] James S.M. Anderson, Maho Nakata, Ryo Igarashi, Katsuki Fujisawa, and Makoto Yamashita. The second-order reduced density matrix method and the two-dimensional hubbard model. *Comp. Theo. Chem.*, 1003(0):22 – 27, 2013.

[2] James F. Annett. Symmetry of the order parameter for high-temperature superconductivity. *Advances in Physics*, 39(2):83–126, 1990.

[3] J. Bardeen, L. N. Cooper, and J. R. Schrieffer. Theory of superconductivity. *Phys. Rev.*, 108:1175–1204, Dec 1957.

[4] E. Brandas and L. J. Dunne. Bardeen-cooper-schrieffer (bcs) theory and yang's concept of off-diagonal long-range order (odlro). *Mol. Phys.*, 112(5-6):694–699, 2014.

[5] A. J. Coleman. Structure of fermion density matrices. *Rev. Mod. Phys.*, 35:668–686, Jul 1963.

[6] A John Coleman. Structure of fermion density matrices. *Rev. Mod. Phys.*, 35(3):668, 1963.

[7] A. John Coleman. The agp model for fermion systems. *Int. J. of Quantum Chem.*, 63(1):23–30, 1997.

[8] Albert John Coleman and Vyacheslav I Yukalov. *Reduced Density Matrices: Coulson's Challenge*, volume 72. Springer Science & Business Media, 2000.

[9] J. Dukelsky, S. Pittel, and G. Sierra. Colloquium. *Rev. Mod. Phys.*, 76:643–662, Aug 2004.

[10] R. M. Erdahl. *Int. J. Quantum Chem*, 13, 1978.

[11] RM Erdahl and B Jin. The lower bound method for reduced density matrices. *Journal of Molecular Structure: THEOCHEM*, 527(1):207–220, 2000.

[12] Claude Garrod and Jerome K. Percus. Reduction of the n-particle variational problem. *J. Math. Phys.*, 5(12):1756–1776, 1964.

[13] Gergely Gidofalvi and David A. Mazziotti. Spin and symmetry adaptation of the variational two-electron reduced-density-matrix method. *Phys. Rev. A*, 72:052505, Nov 2005.

[14] Gergely Gidofalvi and David A. Mazziotti. Computation of quantum phase transitions by reduced-density-matrix mechanics. *Phys. Rev. A*, 74:012501, Jul 2006.

[15] Paolo Giorda and Alberto Anfossi. Structure of quantum correlations in momentum space and off-diagonal long-range order in η pairing and bcs states. *Phys. Rev. A*, 78:012106, Jul 2008.

[16] Osvaldo Goscinski. Antisymmetrized geminal power (agp) wave-functions in finite and extended systems. *Int. J. Quant. Chem.*, 22(S16):591–603, 1982.

[17] Jeff R. Hammond and David A. Mazziotti. Variational two-electron reduced-density-matrix theory: Partial 3-positivity conditions for n-representability. *Phys. Rev. A*, 71(6):062503, June 2005.

[18] Pierre Hohenberg and Walter Kohn. Inhomogeneous electron gas. *Phys. Rev.*, 136(3B):B864, 1964.

[19] J. Hubbard. Electron correlations in narrow energy bands. *Proc. R. Soc. Lond. A*, 276(1365):238–257, November 1963.

[20] Achille Hui and S. Doniach. Penson-kolb-hubbard model: A study of the competition between single-particle and pair hopping in one dimension. *Phys. Rev. B*, 48:2063–2073, Jul 1993.

[21] Yurii A Izyumov. Strongly correlated electrons: the t-j model. *Physics-Uspekhi*, 40(5):445, 1997.

[22] B. Jin. *Quantum Phases for Two-Body Spin-Invariant Nearest Neighbor Interactions*. PhD thesis, 1998.

[23] Gabriel Kotliar. The mott transition and the strong correlation problem. *Physica A: Statistical Mechanics and its Applications*, 280(1):174–184, 2000.

[24] David A Mazziotti. Contracted schrödinger equation: Determining quantum energies and two-particle density matrices without wave functions. *Physical Review A*, 57(6):4219, 1998.

[25] David A Mazziotti. Geminal functional theory: a synthesis of density and density matrix methods. *The Journal of Chemical Physics*, 112(23):10125–10130, 2000.

[26] David A. Mazziotti. Variational two-electron reduced density matrix theory for many-electron atoms and molecules: Implementation of the spin- and symmetry-adapted T_2 condition through first-order semidefinite programming. *Phys. Rev. A*, 72:032510, Sep 2005.

[27] David A. Mazziotti. Structure of fermionic density matrices: Complete n-representability conditions. *Phys. Rev. Lett.*, 108:263002, Jun 2012.

[28] David A. Mazziotti and Robert M. Erdahl. Uncertainty relations and reduced density matrices: Mapping many-body quantum mechanics onto four particles. *Phys. Rev. A*, 63:042113, Mar 2001.

[29] K. A. Penson and M. Kolb. Real-space pairing in fermion systems. *Phys. Rev. B*, 33:1663–1666, Feb 1986.

[30] M. Piris, L. A. Montero, and N. Cruz. The bardeen-cooper-schrieffer approach to electron correlation in the density matrix formalism. *The Journal of Chemical Physics*, 107(1):180–187, 1997.

[31] Marvin E Rensink. Off-diagonal long-range order in the {BCS} theory. *Annals of Physics*, 44(1):105 – 111, 1967.

[32] R. Rodr'iguez-Guzm'an, Carlos A. Jim'enez-Hoyos, R. Schutski, and Gustavo E. Scuseria. Multireference symmetry-projected variational approaches for ground and excited states of the one-dimensional hubbard model. *Phys. Rev. B*, 87:235129, Jun 2013.

[33] Nicholas C. Rubin and David A. Mazziotti. Comparison of one-dimensional and quasi-one-dimensional hubbard models from the variational two-electron reduced-density-matrix method. *Theo. Chem. Acc.*, 133(7), 2014.

[34] Fukashi Sasaki. Eigenvalues of fermion density matrices. *Phys. Rev.*, 138:B1338–B1342, Jun 1965.

[35] Christine A Schwerdtfeger and David A Mazziotti. Convex-set description of quantum phase transitions in the transverse ising model using reduced-density-matrix theory. *J. Chem. Phys.*, 130(22):224102–224102–9, June 2009.

[36] Kuei Sun, Ching-Kai Chiu, Hsiang-Hsuan Hung, and Jiansheng Wu. Tuning between singlet, triplet, and mixed pairing states in an extended hubbard chain. *Phys. Rev. B*, 89:104519, Mar 2014.

[37] C. C. Tsuei and J. R. Kirtley. Pairing symmetry in cuprate superconductors. *Rev. Mod. Phys.*, 72:969–1016, Oct 2000.

[38] Brecht Verstichel, Helen van Aggelen, Ward Poelmans, and Dimitri Van Neck. Variational two-particle density matrix calculation for the hubbard model below half filling using spin-adapted lifting conditions. *Phys. Rev. Lett.*, 108(21):213001, may 2012.

[39] Brecht Verstichel, Helen van Aggelen, Ward Poelmans, Sebastian Wouters, and Dimitri Van Neck. Extensive v2dm study of the one-dimensional hubbard model for large lattice sizes: Exploiting translational invariance and parity. *Comp. Theo. Chem.*, 1003(0):12 – 21, 2013.

[40] Fabian Wenger and Stellan Östlund. d. *Phys. Rev. B*, 47:5977–5983, Mar 1993.

[41] C. N. Yang. Concept of off-diagonal long-range order and the quantum phases of liquid he and of superconductors. *Rev. Mod. Phys.*, 34:694–704, Oct 1962.

[42] Zhengji Zhao, Bastiaan J. Braams, Mituhiro Fukuda, Michael L. Overton, and Jerome K. Percus. The reduced density matrix method for electronic structure calculations and the role of three-index representability conditions. *J. Chem. Phys.*, 120(5):2095–2104, 2004.

CHAPTER 5

CRYSTALLINE-ORBITAL HARTREE-FOCK

In this chapter we present the self-consistent-field method for determining the best linear-combination of crystalline orbitals of an infinite polymer in one-dimension. Crystalline orbital Hartree-Fock (CO-HF) is the extension of molecular orbital theory to an infinite system [6, 1, 8, 2]. As in molecular orbital theory, CO-HF seeks to determine the optimal linear-combination of atomic orbitals for an infinite regular polymer. In position space the interaction operators in the Fock matrix involve infinite summations over the atomic orbitals of the crystal. A super cell with periodic boundaries is imposed by employing a cut off procedure for infinite summations. The super cell serves as a system on which to define a finite set of Bloch orbitals from the Fourier summations of atomic orbitals. The Bloch orbitals naturally obey the underlying translational symmetry of the crystal [9]. Starting from the description of a Bloch orbital we derive the Fock operator in momentum space which will be used in the self-consistent-field procedure. We follow this derivation with an outline of how to apply the direct inversion of the iterative subspace method (DIIS) to the k-space SCF problem. This is followed by the derivation of the one- and two-electron integral tensors in k-space rotated from the Bloch orbital to the crystalline orbital basis for use in post-Hatree-Fock methods. Our derivation follows similar logic and notation to References [13, 10, 19] which outline some of the advancements in post-hartree-fock methods for ground [20, 19, 4, 13, 11], and excited states [14, 16, 5] of periodic systems.

5.1 CO-LCAO-SCF Theory

In CO-HF the wave function is a Slater determinant of Bloch orbitals. The Bloch orbitals are the Fourier sum of atomic orbitals in the entire crystal.

$$\psi_{pk_q}(r) = K^{-1/2} \sum_{\mu} \sum_{m} c_{pk_q}^{\mu k_q} \exp(imk_q a) \chi_\mu(r - m\mathbf{a}) \tag{5.1}$$

The index pk_q is the composite index corresponding to the band p with quasi-momentum index k_q, the sum m is over all unit cell replicas, $\chi_\mu(r - m\mathbf{a})$ represents the atomic orbital basis function in the m^{th} neighboring unit cell, and $c_{pk_q}^{\mu k_q}$ is the coefficient for the crystalline orbital ψ_{pk_q}. Because of the translational symmetry in the crystal the Hartree-Fock equations naturally factor into irreducible representation of the translational group indexed by k_q.

$$\sum_{\nu} f_{\nu k_q}^{\mu k_q} c_{pk_q}^{\nu k_q} = \epsilon_{pk_q} \sum_{\lambda} s_{\lambda k_q}^{\mu k_q} c_{pk_q}^{\lambda k_q} \tag{5.2}$$

The k-space representation of the Fock and overlap matrices in Eq. 5.2 are generated from Fourier summations over their position space representations. This can be derived by considering a general one-particle operator in momentum space expressed as the Fourier summation of its position space representation.

$$\langle pk_p|\hat{O}|qk_q\rangle = \frac{1}{V} \sum_{m_1,m_2=-\infty}^{+\infty} e^{i(m_2 k_q - m_1 k_p)\mathbf{a}} \int \chi_p^*(r - m_1\mathbf{a}) \hat{O} \chi_q(r - m_2\mathbf{a}) \tag{5.3}$$

$$= \frac{1}{V} \sum_{m_1,m_2=-\infty}^{+\infty} e^{i(m_2 - m_1)k_q\mathbf{a}} e^{im_1(k_q - k_p)\mathbf{a}} \int \chi_p^*(r - \mathbf{0a}) \hat{O} \chi_q(r - (m_2 - m_1)\mathbf{a}) \tag{5.4}$$

In Eq. 5.3 the V is the volume of the Brillouin zone, m_1 and m_2 index unit cells of the crystal, and $\mathbf{a}$ is the crystal lattice dimension. The integral in Eq. 5.3 can be rearranged to Eq. 5.4 by exploiting Bloch's theorem to always include the central cell in the integrand.

Because the summations in an infinite system can be rearranged into

$$\sum_{m_1,m_2=-\infty}^{+\infty} \rightarrow \sum_{m_1=-\infty}^{+\infty} \sum_{m_2-m_1=-\infty}^{+\infty} \tag{5.5}$$

without loss of information, we can relax the double summation over the two spatial indices, m_1 and m_2, to a single summation over a new variable $m = m_2 - m_1$ and simplify using the following delta function relation.

$$\sum_{m=-\infty}^{\infty} e^{i(k_q - k_p)m} = 2\pi\delta_{ka}^{k_b} \tag{5.6}$$

We arrive at a formula for the operator $\hat{O}$ in k-space with only one summation of position space integrals.

$$\langle pk_p|\hat{O}|qk_p\rangle = \sum_m e^{ik_p m} \int \chi_p^*(r - \mathbf{0a})\hat{O}\chi_q(r - (m)\mathbf{a}) \tag{5.7}$$

The resolution of the delta function in Eq. 5.6 is also a re-statement of the symmetry requirements that each k_p is the index of an irrep of the translational group. The momentum space description of the Fock and overlap matrices in Eq. 5.8 at each irreducible representation is given as the Fourier sum over the position space Fock and overlap matrices.

$$f_{\nu k_q}^{\mu k_q} = \sum_{m_1=-\infty}^{+\infty} f_{\mu(m_1)}^{\nu(0)} \exp(im_1 k_q a) \tag{5.8}$$

$$s_{\nu k_q}^{\mu k_q} = \sum_{m_1=-\infty}^{+\infty} s_{\mu(m_1)}^{\nu(0)} \exp(im_1 k_q a) \tag{5.9}$$

The AO Fock matrix elements are defined as

$$f^{\nu(0)}_{\mu(m_1)} = h^{\nu(0)}_{\mu(m_1)} + \frac{1}{2}\sum_{\lambda,\kappa}\sum_{m_2=-\infty}^{+\infty}\sum_{m_3=-\infty}^{\infty} p^{\kappa(m_3)}_{\lambda(m_2)} \tag{5.10}$$

$$\times\left(2v^{\mu(0),\lambda(m_2)}_{\nu(m_1),\kappa(m_3)} - v^{\mu(0),\lambda(m_2)}_{\kappa(m_3),\nu(m_1)}\right) \tag{5.11}$$

and the one-, two-electron, and overlap integral tensors in real space are defined in Eqs.(5.12,5.13, 5.14).

$$h^{\nu(0)}_{\mu(m_1)} = \int \chi^*_{\nu(0)}\left(-\frac{1}{2}\nabla^2 - \sum_I \sum_{m_2=-\infty}^{+\infty}\frac{Z_I}{|\mathbf{r}-\mathbf{R}+m_2 a|}\right)\chi_{\mu(m_1)} \tag{5.12}$$

$$v^{\mu(0)\lambda(m_2)}_{\nu(m_1)\kappa(m_3)} = \int\int\left(\chi^{(0)}_{\mu}(r_1)^*\chi^{(m_1)}_{\nu}(r_1)r_{12}^{-1}\chi^{(m_2)}_{\lambda}(r_2)^*\chi^{(m_3)}_{\kappa}(r_2)\right) \tag{5.13}$$

$$s^{\mu(0)}_{\nu(m_1)} = \int \chi^{(0)}_{mu}(r)^*\chi^{m_1}_{\nu}(r) \tag{5.14}$$

Each integral tensor in position space–$f^{\nu(0)}_{\mu(m_1)}$, $h^{\nu(0)}_{\mu(m_1)}$, $h^{\nu(0)}_{\mu(m_1)}$, or $v^{\mu(0)\lambda(m_2)}_{\nu(m_1)\kappa(m_3)}$–can be thought of as a block in a hypermatrix defining the entire crystal in position space [15, 2].

$$H' = \begin{pmatrix} H(0) & H(1) & H(2) & ... & H(N) & ... & H(\infty) \\ H(-1) & H(0) & H(1) & H(2) & ...H(N) & ... & H(\infty-1) \\ \vdots & & & & & & \vdots \\ H(-\infty) & & \cdots & \cdots & H(-2) & H(-1) & H(0) \end{pmatrix} \tag{5.15}$$

Each subblock of the hyper matrix, $H(N)$, corresponds to a integral tensor indexed by m or the analogous two-electron equivalent. Imposing periodic boundaries on the hyper matrix by truncating summations in Eq. 5.10 makes a large cyclic matrix which can always be

diagonalized by a Fourier transform.

5.2 Summation Criteria

We utilize the Namur summation criteria which efficiently exploits the various decay properties of electron densities and has been shown to quickly converge the energy to the thermodynamic limit [22, 12]. The cut off procedure relaxes the infinite summation of m_1, m_2, and m_3 to long-range (L) and short-range (S) summations.

$$\sum_{m_1=-\infty}^{+\infty}\sum_{m_2=-\infty}^{+\infty}\sum_{m_3=-\infty}^{+\infty} \rightarrow \sum_{m_1=-S}^{+S}\sum_{m_2=-L}^{+L}\sum_{m_3=-S+m_2}^{+S+m_2} \tag{5.16}$$

This procedure was developed in conjunction with the multipole expansion technique to treat the long-range interactions neglected by the approximation [7, 3, 13]. This results in the addition of a long-range correction to the total energy (E_{LR}) and a correction to the Fock matrix at each iteration of the SCF procedure. One of the key criteria when selecting the number of unit cells to use in the short-range cut off (S) is the requirement that the density decays to a sufficiently small value by the edge of the super cell. This minimizes any aliasing effects on the density matrix elements when Fourier transformed. These effects have been previously shown to produce instabilities in the exchange field [8] which result in unphysical density matrices with extremely low energies.

Given the truncation procedure the Hartree-Fock energy of the unit cell is defined by

$$\begin{aligned} E =& \sum_{\nu,\mu}\sum_{m=-S}^{S+} p_{\mu(0)}^{\nu(m)} h_{\nu(m)}^{\mu(0)} \\ &+\frac{1}{4}\sum_{\nu,\mu,\lambda,\kappa}\sum_{m_1=-S}^{S+}\sum_{m_2=-L}^{L+}\sum_{m_3=m_2-S}^{m_2+S} p_{\mu(0)}^{\nu(m_1)} p_{\lambda(m_2)}^{\kappa(m_3)} \left(2v_{\nu(m_1)\kappa(m_3)}^{\mu(0)\lambda(m_2)} - v_{\kappa(m_3)\nu(m_1)}^{\mu(0)\lambda(m_2)}\right) \\ &+\frac{1}{2}\sum_{l'}\sum_{A}\sum_{B}\frac{Z_A Z_B}{|\mathbf{R}_A^0 - \mathbf{R}_B^{l'}|} + E_{\mathrm{LR}} \end{aligned} \tag{5.17}$$

where the prime indicates when $l = 0$ $A \neq B$.

5.3 Self-consistent-field iteration and k-space DIIS

The self-consistent-field iteration requires diagonalization of Eq. 5.2 producing new crystal orbitals which are then be used to construct the spatial Fock matrix. The position space density is constructed by the inverse Fourier transform over the orbital coefficients.

$$p^{\kappa(m_3)}_{\lambda(m_2)} = p^{\kappa(m_3-m_3)}_{\lambda(0)} = 2K^{-1} \times \sum_{j}^{\text{occ.}} \sum_{k}^{\text{K}_\text{L}} c^{\kappa k_q}_{jk_q} c^{\lambda k_q *}_{jk_q} \exp(i(m_3 - m_2)k_q a) \tag{5.18}$$

The total self-consistent-field procedure starts with an input position-space density from either diagonalizing the core Hamiltonian or using a superposition of atomic densities in momentum space. The input density is used to construct the Fock matrix in real space which is transformed to momentum-space and diagonalized at each k-point. Using the inverse Fourier transforming in Eq. 5.18 we generate a new position space density to continue the SCF cycle until the density matrices between successive iterations do not change. This

process is described by the flow diagram in Eq. 5.19.

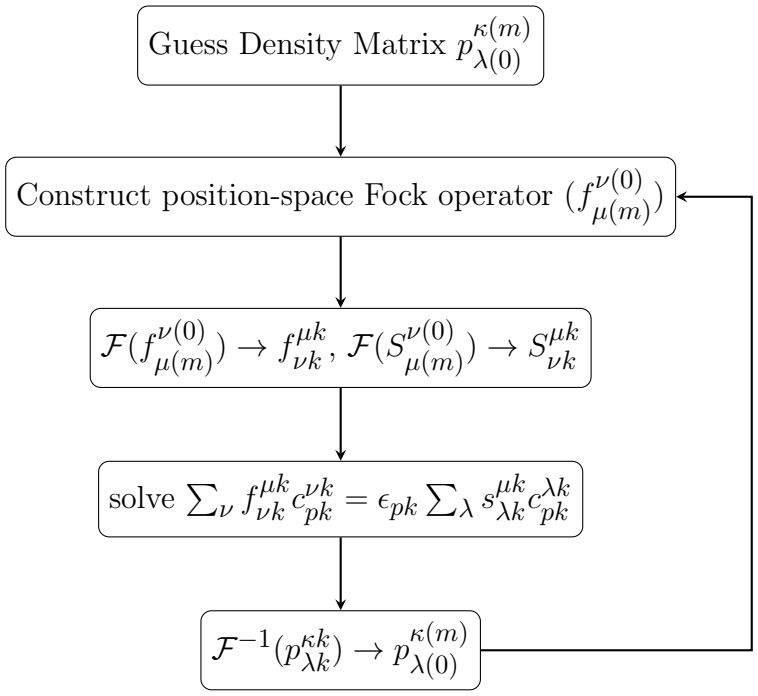

(5.19)

The direct iteration loop in Eq. 5.19 does not always converge to a fixed point. There are several ways to ensure convergence, such as damping and level shifting, when the direct iteration method does not yield a stationary solution. The most popular of these is the direct inversion in the iterative subspace method (DIIS) by Pulay [17, 18]. The DIIS method generates the density matrix for the next iteration by using a linear combination of previous density matrices.

$$D_{ij}(k)_{n+1} = \sum_i^m c_i D_{ij}(k)_i \tag{5.20}$$

$$\sum_i^m c_i = 1 \tag{5.21}$$

Accordingly, the corresponding error vector for the interpolated $n+1$ density matrix is a linear combination of previous error vectors.

$$e_{n+1} = \sum_{i}^{m} c_i e_i \tag{5.22}$$

The coefficient c_i is selected such that they minimize the norm of error vectors between successive iterations.

$$L = ||e_{n+1}||^2 - \lambda(\sum_{i}^{m} -1) \tag{5.23}$$

$$= \sum_{ij} c_i B_{ij} c_j - \lambda(\sum_{i}^{m} c_i - 1) \quad , \quad \text{where} B_{ij} = \langle e_i | e_j \rangle \tag{5.24}$$

There are many choices of what to uses as the error vector. The error vector determined by Pulay for specific use in the Roothan-Hartree-Fock procedure is given in Eq. (5.25)

$$e(k)_{i+1} = \sum_{i} c_i (F(k)_i, D(k)_i S(k) - S(k) D(k)_i F(k)_i) \tag{5.25}$$

The normalization of the coefficients $\{c_i\}$ restrict the interpolated density matrix to be within the affine subspace of prior density matrices. We apply the DIIS procedure to all the k-space density matrices and solve the DIIS least-squares problem for each k-point separately.

5.4 Building ${}^2V(k)$ and ${}^1h(k)$

The one- and two-electron integral tensors are rotated into the crystalline orbital basis for post-mean-field methods. Given the structure of the Bloch orbitals in Eq. (5.1) the two-electron integrals in the crystalline orbital basis are defined as the two-dimensional Fourier

transform over real-space two-electron integrals.

$$\langle pk_pqk_q||rk_rsk_s\rangle = K^{-2}\sum_{\mu,\nu,\kappa,\lambda}\sum_{m_1,m_2,m_3,m_4} c^{\mu k_p *}_{pk_p} c^{\lambda k_q *}_{qk_q} c^{\nu k_r}_{rk_r} c^{\kappa k_s}_{sk_s} \langle \mu^{m_1}\lambda^{m_2}||\nu^{m_3}\kappa^{m_4}\rangle$$
$$\times \exp\left(i\left(-m_1k_p - m_2k_q + m_3k_r + m_4k_s\right)\right) \tag{5.26}$$

One of the indices is removed by substituting one summation over m for a Kronecker delta

$$\langle pk_pqk_q||rk_rsk_s\rangle = K^{-1}\sum_{\mu,\nu,\kappa,\lambda}\sum_{m_1^{'},m_2^{'},m_3^{'},} c^{\mu k_p *}_{pk_p} c^{\lambda k_q *}_{qk_q} c^{\nu k_r}_{rk_r} c^{\kappa k_s}_{sk_s} \langle \mu^{0}\lambda^{m_2^{'}}||\nu^{m_1^{'}}\kappa^{m_3^{'}}\rangle \tag{5.27}$$
$$\times \exp\left(i\left(-m_2^{'}k_q + m_1^{'}k_r + m_3^{'}k_s\right)a\right) \tag{5.28}$$

where the only k-space integrals that survive are zero momentum transfer

$$(k_p + k_q - k_r - k_s)\mathbf{a}\%2\pi = 0. \tag{5.29}$$

Substituting the infinite lattice sums for the Namur summation results in an expression for the two-electron integral tensor in the crystal orbital basis.

$$\langle pk_pqk_q||rk_rsk_s\rangle = K^{-1}\sum_{\mu,\nu,\kappa,\lambda}\sum_{m_1^{'}=-S}^{+S}\sum_{m_2^{'}=-L}^{+L}\sum_{m_3^{'}=m_2^{'}-S}^{m_2^{'}+S} c^{\mu k_p *}_{pk_p} c^{\lambda k_q *}_{qk_q} c^{\nu k_r}_{rk_r} c^{\kappa k_s}_{sk_s} \langle \mu^{0}\lambda^{m_2^{'}}||\nu^{m_1^{'}}\kappa^{m_3^{'}}\rangle$$
$$\times \exp\left(i\left(-m_2^{'}k_q + m_1^{'}k_r + m_3^{'}k_s\right)a\right) \tag{5.30}$$

The Namur cut off criteria and the approximate (infinite) Fourier transform introduce asymmetries into the one- and two-electron integral structure. As a result we enforce the four-fold complex valued two-electron integral symmetry.

$$\langle ij||kl\rangle = \langle ji||lk\rangle = \langle kl||ij\rangle^* = \langle lk||ji\rangle^* \tag{5.31}$$

The four-fold symmetry for complex valued two-electron integrals [21] is raised to the normal eight-fold symmetry by time reversal symmetry discussed in Chapter 5. The one-electron integral tensor in the Bloch basis $H(k)$ can be rotated to the crystalline-orbital basis $h(k)$ in the usual manner.

$$h(k) = C(k)^{\dagger} H(k) C(k) \tag{5.32}$$

The long range interactions from the multipole expansion are included at the one-electron level. The additional terms added to the real-space one-electron terms are Fourier transformed and rotated to the crystalline orbital basis in the same fashion as the normal one-electron pieces. This procedure can be viewed as creating a new effective one-body Hamiltonian that includes some long-range interaction.

5.5 References

[1] Jean Marie André. Self-consistent field theory for the electronic structure of polymers. *J Chem. Phys.*, 50(4):1536–1542, 1969.

[2] Jean-Marie André, Joseph Delhalle, and Janos Ladik. *Quantum Theory of Polymers: Proceedings of the NATO Advanced Study Institute on Electronic Structure and Properties of Polymers Held at Namur, Belgium, 31 August–14 September, 1977*, volume 39. Springer Science & Business Media, 2012.

[3] JM André, DP Vercauteren, VP Bodart, and JG Fripiat. Ab initio calculations of the electronic structure of helical polymers. *J Comp. Chem.*, 5(6):535–547, 1984.

[4] Philippe Y. Ayala, Konstantin N. Kudin, and Gustavo E. Scuseria. Atomic orbital laplace-transformed second-order moller-plesset theory for periodic systems. *J. Chem. Phys.*, 115(21):9698–9707, 2001.

[5] Viktor Bezugly and Uwe Birkenheuer. Multireference configuration interaction treatment of excited-state electron correlation in periodic systems: the band structure of trans-polyacetylene. *Chem. Phys. Lett.*, 399(1):57 – 61, 2004.

[6] G. Del Re, J. Ladik, and G. Biczó. Self-consistent-field tight-binding treatment of polymers. i. infinite three-dimensional case. *Phys. Rev.*, 155:997–1003, Mar 1967.

[7] Joseph Delhalle, Lucjan Piela, Jean-Luc Brédas, and Jean-Marie André. Multipole expansion in tight-binding hartree-fock calculations for infinite model polymers. *Phys. Rev. B*, 22:6254–6267, Dec 1980.

[8] R Dovesi, C Pisani, and C Roetti. Hartree-fock ab initio treatment of crystalline systems. *Lecture Notes in Chemistry*, 48, 1988.

[9] Robert A Evarestov. *Quantum chemistry of solids: the LCAO first principles treatment of crystals*, volume 153. Springer Science & Business Media, 2007.

[10] So Hirata. Quantum chemistry of macromolecules and solids. *Phys. Chem. Chem. Phys.*, 11:8397–8412, 2009.

[11] So Hirata, Ireneusz Grabowski, Motoi Tobita, and Rodney J. Bartlett. Highly accurate treatment of electron correlation in polymers: coupled-cluster and many-body perturbation theories. *Chem. Phys. Lett.*, 345(5):475 – 480, 2001.

[12] So Hirata and Yu-ya Ohnishi. Thermodynamic limit of the energy density in a crystal. *Phys. Chem. Chem. Phys.*, 14:7800–7808, 2012.

[13] So Hirata, Rafał Podeszwa, Motoi Tobita, and Rodney J. Bartlett. Coupled-cluster singles and doubles for extended systems. *J. Chem. Phys.*, 120(6):2581–2592, 2004.

[14] Hideki Katagiri. Equation-of-motion coupled-cluster study on exciton states of polyethylene with periodic boundary condition. *J. Chem. Phys.*, 122(22), 2005.

[15] J. Ladik. *Electronic structure of polymers and molecular crystals*, volume 9. Springer Science & Business Media, 2013.

[16] Ramiro Pino and Gustavo E. Scuseria. Laplace-transformed diagonal dyson correction to quasiparticle energies in periodic systems. *J. Chem. Phys.*, 121(6):2553–2557, 2004.

[17] Peter Pulay. Convergence acceleration of iterative sequences. the case of scf iteration. *Chem. Phys. Lett.*, 73(2):393–398, 1980.

[18] Thorsten Rohwedder and Reinhold Schneider. An analysis for the diis acceleration method used in quantum chemistry calculations. *J. Math. Chem.*, 49(9):1889–1914, 2011.

[19] Jun-Qiang Sun and Rodney J. Bartlett. Second-order many-body perturbation theory calculations in extended systems. *J. Chem. Phys.*, 104(21):8553–8565, 1996.

[20] Jun-Qiang Sun and Rodney J. Bartlett. Convergence of many-body perturbation methods with lattice summations in extended systems. *J. Chem. Phys.*, 106(13):5554–5563, 1997.

[21] Attila Szabo and Neil S Ostlund. *Modern quantum chemistry: introduction to advanced electronic structure theory*. Courier Corporation, 2012.

[22] Hiroyuki Teramae. Study on the behavior of energy convergence in ab initio crystal orbital calculations. *Theo. Chem. Acc.*, 94(6):311–331, 1996.

CHAPTER 6

NECESSARY N-REPRESENTABILITY CONSTRAINTS FROM TIME-REVERSAL SYMMETRY FOR EXTENDED SYSTEMS

This chapter contains parts of work in preparation [N. C. Rubin and D. A. Mazziotti (*in preparation*, 2016)].

6.1 Overview

In this chapter we formulate the variational 2-RDM method for systems with periodic boundaries. The structure of the 2-positivity constraints are derived considering translational and time-reversal invariance of the Hamiltonian. Enforcement of time-reversal (TR) symmetry augments the p-positive non-negativity constraints with additional equalities between Kramers pairs of one- and two-particle density matrices. Time-reversal symmetry is implicitly included when real valued spatial spin-orbitals are spin-adapted into basis functions satisfying the S^2 and S_z operators[4, 10]. For a complex valued wave function in a momentum space basis the time-reversal operator negates the spin and basis momentum expectation values. Therefore, the time-reversal constraint is no longer implicitly included upon spin-adapting. We derive the equalities from TR symmetry for general one- and two-body operators. These constraints are demonstrated to be necessary when considering a complex valued k-space Hamiltonian that is time-reversal invariant and has translational symmetry. Without the TR constraints the variational 2-RDM method produces energies significantly below the true ground state energy.

Time-reversal symmetry has been previously used as a tool in solving N-representability by determining the structure of natural orbitals and natural geminals of the the one- and two-body density matrices. The structure was used to demonstrate the pair-wise degeneracy of natural orbital occupations of the 1-RDM [16] for even N systems with non-degenerate

and degenerate states [5]. For time-reversal invariant Hamiltonians with translational symmetry there is a natural degeneracy between $(k, -k)$ wave-functions. Using the $(k, -k)$ single particle functions, a real valued basis set can be formed by taking linear combinations between the pairs. The real valued functions are then easily spin-adapted to form a TR invariant basis [5, 14]. Unfortunately, this symmetry adapting destroys the advantageous block diagonal structure of the Hamiltonian necessary for efficient computational performance. In variational RDM theory we can keep the advantageous k-space blocking structure and add TR-symmetry constraints as equalities on the density matrices during the energy minimization, without destroying the 1- and 2-RDM's block diagonal structure.

6.2 Variational 2-RDM Theory With Periodic Boundaries

In variational 2-RDM theory on extended systems the reduced Hamiltonian and density matrix are blocked according to the irreducible representations of the translation operator [7, 2]. The reduced Hamiltonian is expressed as

$$\begin{aligned} {}^2K^{ak_a,bk_b}_{ik_i,jk_j} =& \frac{1}{(K_L \times N) - 1} \left(\delta^{ak_a}_{ik_i} h^{bk_b}_{jk_j} \hat{a}^\dagger_{jk_j} \hat{a}_{bk_b} + \delta^{bk_b}_{jk_j} h^{ak_a}_{ik_k} \hat{a}^\dagger_{ak_a} \hat{a}_{ik_i} \right) \\ &+ V^{ak_a,bk_b}_{ik_i,jk_j} \hat{a}^\dagger_{ak_a} \hat{a}^\dagger_{bk_b} \hat{a}_{jk_j} \hat{a}_{ik_i} \end{aligned} \tag{6.1}$$

where the indices are composite indices representing the band index and quasi-momentum index k, K_L is the number of k-points sampled, $\hat{a}^\dagger$ ($\hat{a}$) are Fermionic creation (annihilation) operators, and $h^{bk_b}_{jk_j}$ and $V^{ak_a,bk_b}_{ik_i,jk_j}$ are the one- and two-electron integral tensors in the crystalline orbital basis. The Hamiltonian is non-zero wherever $(k_i + k_j - k_a - k_b) \mathrm{mod}(2\pi) = 0$ is satisfied. The metric matrices all have the same blocking structure as they must share the symmetries supported by the Hamiltonian. In momentum space the structure of the p-positivity constraints remain the same as position space. These constraints restrict the

$(p+1)$ metric (or overlap) matrices of the form

$$M_k = \langle\psi|\hat{C}_k{}^\dagger \hat{C}_k|\psi\rangle \tag{6.2}$$

to be positive semidefinite. The operator $\hat{C}_k$, represents the set of p-particle operators of momentum k that form the p-particle basis functions from which the overlap matrix is obtained. Considering rank-2 polynomials of creation annihilation operators in Eq. [6.3] and substituting into Eq. [6.2] we generate a set of metric matrices which constrain the k-dependent probability distribution of finding two particles, two-holes, and a particle-hole pair to be positive semidefinite.

$$\begin{aligned}
\hat{C}_{D_k} &= \hat{a}^\dagger_{jk_a}\hat{a}^\dagger_{ik_b} \quad (k_a + k_b)\mathrm{mod}(2\pi) = k \\
\hat{C}_{Q_k} &= \hat{a}_{jk_a}\hat{a}_{ik_b} \quad (-k_a - k_b)\mathrm{mod}(2\pi) = k \\
\hat{C}_{G_k} &= \hat{a}^\dagger_{jk_a}\hat{a}_{ik_b} \quad (k_a - k_b)\mathrm{mod}(2\pi) = k
\end{aligned} \tag{6.3}$$

The indices in Eq. [6.3] are composite indices corresponding to a band and momentum index. The computational implementation of the variational energy minimization with respect to the 2-RDM is formulated in the usual way as a *semidefinite program* (SDP). The program is constructed by considering the minimization of the linear energy functional, Eq. [6.4]

$$E = \mathrm{Tr}[{}^2K \cdot {}^2D] \tag{6.4}$$

subject to the following constraints:

$$AX = b \quad X \succeq 0. \tag{6.5}$$

$X \succeq 0$ is the block representation of the reduced density matrices in Eq. (6.6) constrained to be positive semidefinite.

$$X = \sum_k \oplus \begin{pmatrix} {}^1D_k & 0 & 0 & 0 & 0 \\ 0 & {}^1Q_k & 0 & 0 & 0 \\ 0 & 0 & {}^2D_k & 0 & 0 \\ 0 & 0 & 0 & {}^2Q_k & 0 \\ 0 & 0 & 0 & 0 & {}^2G_k \end{pmatrix} \tag{6.6}$$

The A matrix in Eq. (6.5) contains the mapping relation between each p-particle metric matrix.

6.3 Time-Reversal Equality Constraints

An operator that is invariant under a symmetry operation g necessarily obeys the following similarity transform.

$$[g, \hat{O}] = 0 \quad g\hat{O}g^{-1} = \hat{O} \tag{6.7}$$

The eigenstates of $\hat{O}$ can be chosen to be simultaneous eigenstates of g. The similarity transform can be represented by the Baker-Campbell-Hausdorff transformation, which implies the constraints on $\hat{O}$ by $[\hat{O}, i\hat{S}] = 0$.

$$e^{i\hat{S}}\hat{O}e^{-i\hat{S}} = \hat{O} + [\hat{O}, i\hat{S}] + \frac{1}{2!}[[\hat{O}, i\hat{S}], i\hat{S}] + \cdots \tag{6.8}$$

For example, the Fock operator that is invariant to S^2 and S_z implies a restricted form of the Fock operator where $F_{\alpha,\alpha} = F_{\beta,\beta}$ [6, 17].

We augment the equality constraints on the 2-RDM by enforcing the equivalency of

$(k, -k)$ metric matrices. These equalities are derived by considering the similarity transform of the one- and two-body metric matrices with the time-reversal symmetry operator. The TR operator is written as a product of a unitary operator and the complex conjugation operator with respect to a particular basis.

$$\Theta = UK \tag{6.9}$$

The U operator is the finite rotation around y-axis in spin-space by $\pi/2$ such that it anti-commutes with σ_x and σ_z.

$$U = \exp\left(-i\pi\ {}^{N}S_y\right) \tag{6.10}$$

The similarity transform of a S^2 spin adapted operator dictates the restrictions between particular k states.

$$\begin{pmatrix} 0 & 1 \\ -1 & 0 \end{pmatrix} K \begin{pmatrix} O^{\rightarrow}_{k,\alpha,\alpha} & 0 \\ 0 & \hat{O}^{\rightarrow}_{k,\beta,\beta} \end{pmatrix} K^{\dagger} \begin{pmatrix} 0 & 1 \\ -1 & 0 \end{pmatrix}^{-1} = \tag{6.11}$$

$$\begin{pmatrix} O^{*\rightarrow}_{-k,\beta,\beta} & 0 \\ 0 & O^{*\rightarrow}_{-k,\alpha,\alpha} \end{pmatrix} = \begin{pmatrix} O^{*\rightarrow}_{-k,\alpha,\alpha} & 0 \\ 0 & O^{*\rightarrow}_{-k,\beta,\beta} \end{pmatrix} \tag{6.12}$$

The second equality comes from the spin restriction requiring α and β spin orbitals to be equal. For the 1-particle and 1-hole density matrices we explicitly include the following relation in the A matrix

$$\Theta({}^{1}D^{k}_{ij})\Theta^{-1} = [{}^{1}D^{-k}_{ij}]^{*} \tag{6.13}$$

$$\Theta({}^1Q^k_{ij})\Theta^{-1} = [{}^1Q^{-k}_{ij}]^* \tag{6.14}$$

Unlike in position space where time-reversal symmetry forces the one-body operator to be real-valued [6] in a spin-adapted basis set, a general complex momentum space one-body operator can be complex valued as long as the matrix blocks corresponding to $(k, -k)$ pairs are complex conjugates of each other.

The constraints on the two-body density matrices are determined by applying the time-reversal similarity transform to each $\hat{C}$ operator.

$$\langle\psi|\Theta\hat{C}_{ij}\Theta^{-1}\Theta\hat{C}^\dagger_{ab}\Theta^{-1}|\psi\rangle \tag{6.15}$$

This results in the following equalities for each $(k, -k)$ block in the 2-particle metric matrices:

$${}^2M_{i\alpha,j\beta;k\alpha,l\beta}(k) = \Big[\,{}^2M_{i\beta,j\alpha;,k\beta,l\alpha}(-k)\Big]^* \tag{6.16}$$

where $M = D, Q, G$. The similarity transform of spin-adapted $\hat{C}$ operators result in a equivalency between $(k, -k)$ blocks of the singlet and triplet parts of each metric matrix [15, 7]. A consequence of the above symmetries is that the $k = 0$ and $k = \pi$ blocks must be real valued on the one- and two-particle space. Using the normal p-positive set, commonly denoted DQG, and including the time-reversal constraints generate the approximate N-representability constraints used in this work. All calculations using this set are labeled RDM-TR. We compare the augmented N-representability constraints against normal 2-positivity without the time-reversal equalities which are labeled RDM [8].

In the SDP the complex valued k-space density matrices are represented by $2N \times 2N$ real matrices where N is the linear dimension of the k-space matrix [12]. The TR equality constraints manifest themselves differently for symmetric or anitsymmetic matrices. The TR operator maps a geminal to its time-reversed pair $(ik_i, jk_j) \rightarrow (i\overline{k_i}, j\overline{k_j})$, where $\overline{k_i} = -k_i$.

For singlet matrices the exchange of indices is symmetric and so each element of the $(k, -k)$ matrices are complex conjugate each other. For triplet matrices the exchange of indices is antisymmetric and thus occasionally the TR operator maps a geminal to its negative. In this case particular $(k, -k)$ block elements are necessarily zero.

6.4 Applications

We test these constraints by calculating the binding energies of two one-dimensional polymers. Each polymer is first described at the mean-field level with crystalline orbital Hartree-Fock (CO-HF) [11, 3]. CO-HF performs Hartree-Fock on a set of non-orthogonal bloch vectors built by Fourier summation of atomic orbitals over a super-cell. The complex-valued crystalline orbitals are used to build the one- and two-electron integral tensors in k-space [18], which are subsequently used to build the reduced-Hamiltonian. The CO-HF calculation performs a lattice truncation asymmetrically resulting in the destruction of the four-fold two-electron integral symmetry [19, 11]. This symmetry along with the time-reversal symmetry for each k-point is explicitly restored when building the reduced Hamiltonian prior to the calculation. This is accomplished by explicitly building the two-electron integral tensor with eight-fold symmetry–four from the integrals times two from time-reversal.

For variational minimization of the energy with respect to the 2-RDM subject to 2-positivity conditions that are not augmented with the time-reversal symmetry constraints we find the calculations are either i) not able to find a ground state solution or ii) converge to a 2-RDM with broken TR symmetry. This results in an energy that is below the true ground state energy.

The first system we consider is the binding of an infinite hydrogen chain. We compare the energies from CO-HF, MP2, variational RDM with DQG constraints and variational RDM with DQG + time-reversal equality constraints around the chains binding minimum.

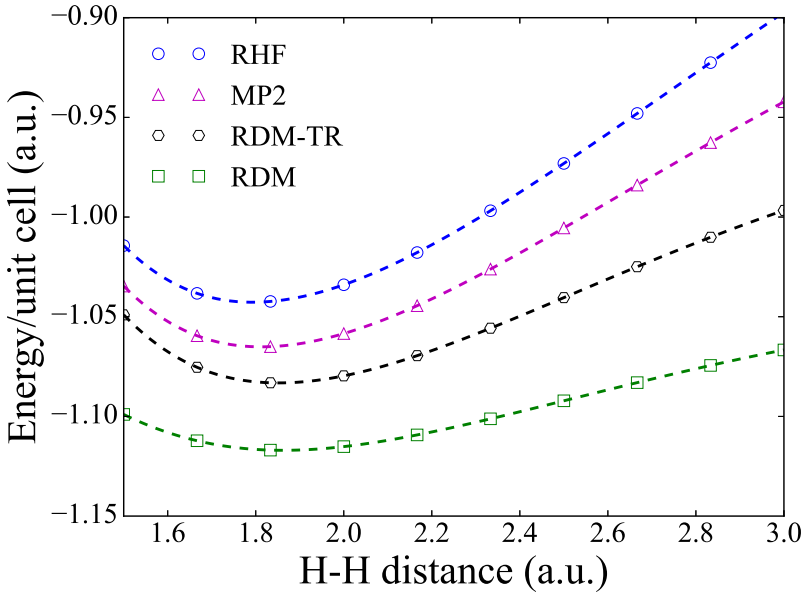

Figure 6.1: $(H_2)_\infty$ computed at RHF, MP2, RDM, and RDM-TR. The RDM-TR curve is indistinguishable from a 50 atom DMRG calculation found in Ref. [9].

For the crystalline orbital Hartree-Fock we use a unit cell of two Hydrogen atoms and set the short and long range cut off criteria to be 10. We sample k-space at 20 evenly spaced points. Møller-Plesset perturbation theory for the periodic system is implemented based on Ref. [18, 11]. It has been previously demonstrated that correlations in hydrogen chains cause the density matrix elements to decay extremely slowly with respect to the central unit cell [20]. Despite this, their energies and properties, such as conduction, converge extremely rapidly with respect to chain size [1]. Therefore, we can evaluate the efficacy of the k-space variational 2-RDM method by evaluating the accuracy of the Hydrogen chain at the dissociated limit and the binding minimum by comparing the energy of PBC calculations against the energy for analogous large-scale finite chains with open boundary condition. We plot the energies in Fig. [6.1] for the four aforementioned methods. MP2 shows good improvement over the Hartree-Fock solution but is known to diverge as the system becomes more correlated. The energy determined by variational 2-RDM theory with normal 2-positivity constraints results in a lower bound of approximately 50 milliHartrees for the entire binding

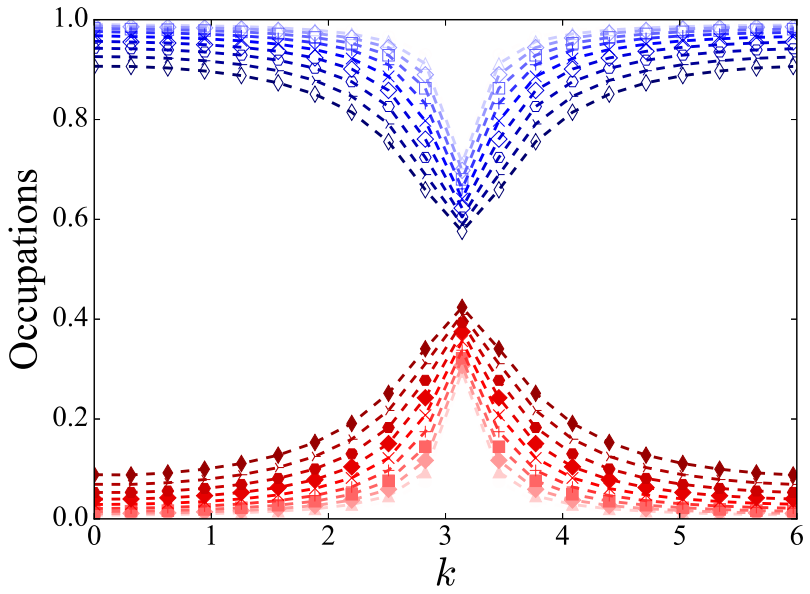

Figure 6.2: Occupation numbers of RDM with time-reversal symmetry. Symmetric around π and approaching the correct completely dialated lattice values of 0.5. Blue curves are the HONO occupations and red curves are LUNO occupations. The darker the curve indicates a more dilated lattice.

region of the Hydrogen chain. When the additional time-reversal symmetry constraints are added to the SDP we recover a solution that corresponds with large-scale open boundary condition calculations for the entire binding region.

Time-reversal symmetry dictates a degeneracy in the density matrices and thus eigenvalues at the 1- and 2-particle level[16, 5]. In Fig. [6.3] we compare the occupation numbers for each band at each k-point for two metallic solutions. The variational RDM calculation that is un-augmented with TR constraints produces occupations that are not only asymmetric around π but also artificially large. When TR equality constraints are added the occupations are symmetric around π as expected. Fig. [6.2] is a plot of all the k-point occupations for the dilation of the Hydrogen chain. We see that as we approach the dilated limit the occupations approach the physically correct value of 0.5.

In many cases it is unnecessary to correlate core electrons. For the binding curves of the Lithium Hydride chain we consider an active space of bands around the Fermi surface.

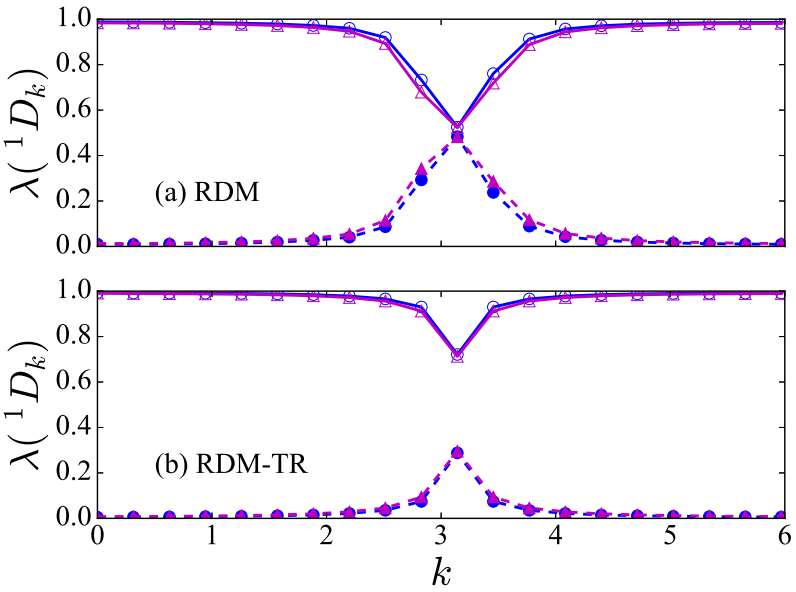

Figure 6.3: Metallic solution k-dependent occupation numbers at points 0 and point 1 (1.5 bohr and 1.666 bohr separation of hydrogen atoms in the chain) on the binding scan above at the RDM level. The top (a) is no time-reversal symmetry. The bottom (b) is time-reversal symmetry restored. The restoration of the symmetry enforces the correct density matrix symmetry around π.

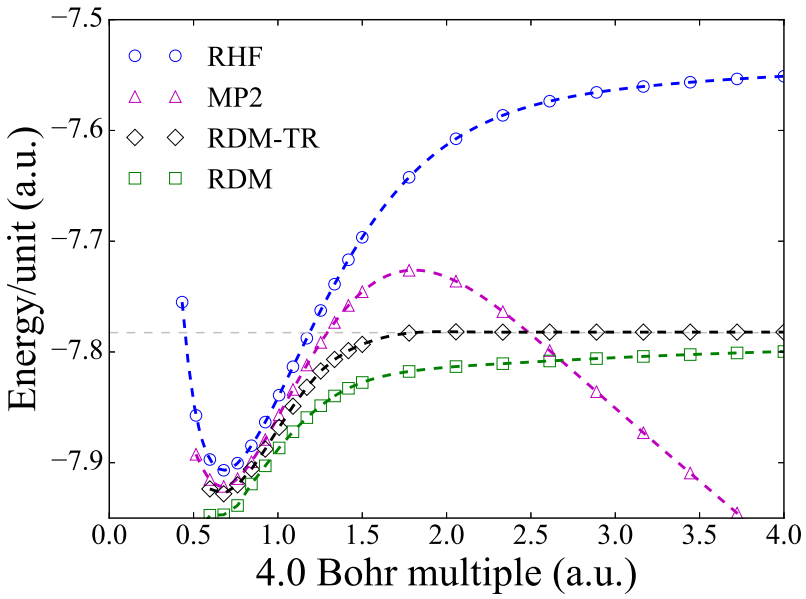

Figure 6.4: $(LiH)_\infty$ computed with RHF, MP2, and RDM . The RDM calculation with and without time-reversal symmetry N-representability three active bands. The grey line is a $(LiH)_6$ dilated to its dissociated limit.

The active space Hamiltonian treats core electrons at the mean-field level without relying on pseudo-potentials for the valence [13]. We selected all bands involving significant character on the frontier orbitals of the unit cell. With just three bands in the active space we are able to capture the correct dissociation character of the Lithium Hydride crystal. The Lithium Hydride crystal was built by considering a single Lithium Hydride in the unit cell with five neighboring cells. The Li-H distance was 4.0 Bohr while the H-Li distance was 6.0 Bohr. The crystal dilation was performed by multiplying the internal bond lengths by a scalar referenced in Fig. [6.4]. Even on a small active space we see that time-reversal constraints are necessary to accurately describing the binding of LiH. Without the TR-equality constraints the RDM solutions lower bounds the correct solution throughout the binding region by a significant amount.

6.5 Conclusion

We derived the structure of p-positivity conditions for a general multi-band Hamiltonian describing a periodic system. We determined that though time-reversal invariance is implicitly included in real-valued spin-adapted density matrices explicit equality constraints are necessary for the more general complex valued time-reversal invariant Hamiltonians. The equality constraints arise naturally between Kramers pairs of one- and two-particle density matrices along with restricting particular imaginary parts to be zero upon spin-adapting. Though the complex piece of the 2-RDM can be removed by taking linear combinations of Kramers pairs of basis functions the process destroys the advantageous block-diagonal structure of the Hamiltonian. The time-reversal constraints are added to the semidefinite program and optimized implicitly. The necessity of these equality constraints is demonstrated by calculating occupation numbers and binding energies on two paradigmatic strongly correlated infinite systems.

Accurately calculating the correlated ground state electronic structure of bulk and extended systems is an important step moving past model Hamiltonians for understanding correlation driven phenomenon. The variational 2-RDM methodology provides the theoretical and computational framework for efficiently simulating these extended systems. Coupled with a local basis approach from crystalline-orbital Hartree-Fock all of the normal quantum chemical analysis tools, such as Mulliken populations, dipole and quadrupole expectation values in the unit cell, are easily computable with the 1- and 2-RDMs. The necessary constraints on the 2-RDM with approximate N-representability can now be used in extendeding other reduced-density matrix methodologies such as parametric-RDM and the AntiHermetian Contracted Schrödinger Equation method to study extended systems.

6.6 References

[1] Gian Luigi Bendazzoli, Stefano Evangelisti, and Antonio Monari. Full-configuration-interaction study of the metal-insulator transition in a model system: Hn linear chains n=4, 6,$\cdots$, 16. *I. J. Quant. Chem.*, 111(13):3416–3423, 2011.

[2] F Albert Cotton. *Chemical applications of group theory*. John Wiley & Sons, 2008.

[3] R Dovesi, C Pisani, and C Roetti. Hartree-fock ab initio treatment of crystalline systems. *Lecture Notes in Chemistry*, 48, 1988.

[4] Knut Faegri Jr and K. Dyall. *Introduction to relativistic quantum chemistry*. Oxford University Press, USA, 2007.

[5] Karl F. Freed. N representability of fermion density matrices. *J. Chem. Phys.*, 47(10):3907–3911, 1967.

[6] Hideo Fukutome. Unrestricted hartree–fock theory and its applications to molecules and chemical reactions. *International Journal of Quantum Chemistry*, 20(5):955–1065, 1981.

[7] Gergely Gidofalvi and David A. Mazziotti. Spin and symmetry adaptation of the variational two-electron reduced-density-matrix method. *Phys. Rev. A*, 72:052505, Nov 2005.

[8] Gergely Gidofalvi and David A. Mazziotti. Molecular properties from variational reduced-density-matrix theory with three-particle n-representability conditions. *J. Chem. Phys.*, 126(2), 2007.

[9] Johannes Hachmann, Wim Cardoen, and Garnet Kin-Lic Chan. Multireference correlation in long molecules with the quadratic scaling density matrix renormalization group. *J. Chem. Phys.*, 125(14):–, 2006.

[10] Trygve Helgaker, Poul Jorgensen, and Jeppe Olsen. *Molecular electronic-structure theory*. John Wiley & Sons, 2014.

[11] So Hirata, Rafał Podeszwa, Motoi Tobita, and Rodney J. Bartlett. Coupled-cluster singles and doubles for extended systems. *J. Chem. Phys.*, 120(6):2581–2592, 2004.

[12] M. W. Hirsch and S. Smale. *Differential Equations, Dynamical Systems, and Linear Algebra*. Academic, 1974.

[13] R. P. Hosteny, T. H. Dunning, R. R. Gilman, A. Pipano, and I. Shavitt. Ab initio study of the π-electron states of trans-butadiene. *J. Chem. Phys.*, 62(12):4764–4779, 1975.

[14] Richard M. Martin. *Electronic Structure: Basic Theory and Practical Methods*. Cambridge University Press, 2004.

[15] Jun John Sakurai and Jim J Napolitano. *Modern Quantum Mechanics*. Pearson Higher Ed, 2014.

[16] Darwin W. Smith. n-representability problem for fermion density matrices. ii. the first-order density matrix with n even. *Phys. Rev.*, 147:896–898, Jul 1966.

[17] JL Stuber and J Paldus. Symmetry breaking in the independent particle model. *Fundamental World of Quantum Chemistry, A Tribute Volume to the Memory of Per-Olov Löwdin*, 1:67–139, 2003.

[18] Jun-Qiang Sun and Rodney J. Bartlett. Second-order many0body perturbation-theory calculations in extended systems. *J. Chem. Phys.*, 104(21):8553–8565, 1996.

[19] Attila Szabo and Neil S Ostlund. *Modern quantum chemistry: introduction to advanced electronic structure theory*. Courier Corporation, 2012.

[20] Tomonori Yamada, Ryan P. Brewster, and So Hirata. Asymptotic expansion of two-electron integrals and its application to coulomb and exchange lattice sums in metallic, semimetallic, and nonmetallic crystals. *J. Chem. Phys.*, 139(18), 2013.

CHAPTER 7

CONCLUDING REMARKS

7.1 The variational 2-RDM method

The variational 2-RDM method is an extremely robust methodology for capturing strong correlation. It is a reference free method and has polynomial scaling in computational size and solver convergence. Furthermore, the 2-RDM is sufficient for calculating the expectation value of any two-body operator. The only drawback is the lack of characterization of the 2-cone over which the 2-RDM is minimized. This means that any 2-RDM ground state determined using approximate N-representability is necessarily a lower bound to the exact solution. It is clear by the conclusion of this thesis and the impressive work of others testing the bounds of approximate N-representability for a variety of lattice models in the strong correlation limit [14, 13, 1] that the approximate 3-positive N-representability constraints are sufficient for chemical accuracy in almost all situations. In some sense this is the conclusion of the search for a solution to the N-representability problem originally put for by Coulson more than 50 years ago [4]. A constructive solution has also been formulated [8, 9] but tighter constraints on the 2-cone seem hardly necessary considering their cost. But this is not the end of studying approximate N-representability. In Chapter 4 a superconducting Hamiltonian that projected out η-pairing wave functions was studied. Hidden there was the possibility of using a simplified wave function ansatz to further reduce the size and structure of the metric-matrices. Recent work by Poelmans *et. al.* in using this double-occupation restriction on the wave function demonstrates the possibility for combining structured wave function techniques to inform N-representability choice [12]. It is my belief that the next frontier of the variational 2-RDM method will involve efficient approximations to N-representability, improvements in its computational implementations, and applications to novel systems.

7.2 Periodic systems

The 2-RDM is an extremely elegant and compact representation of all the necessary information required to calculate the ground state energy of a quantum system. As such, its natural extension to systems with periodicity is not surprising. In fact, because the 2-RDM naturally reflects the underlying symmetry of a translationally invariant system all metric matrices become block diagonal, which adds to the computational advantage of the method. Careful application of the positivity conditions to new systems will be central to growing the 2-RDM methodology. In this work we have developed the necessary formalism for 2-RDM calculations on periodic systems. Special consideration for implied symmetries, such as time-reversal symmetry, must always be included in the N-representability conditions on the 2-RDM and its associated metric matrices. With this in mind, extending these constraints to other RDM methods such as the parametric-RDM and the Antihermetian Contracted Schrödinger Equation (ACSE) method is a route to easily obtain excited states and describe larger systems.

7.3 Semidefinite programming

The variational 2-RDM method has greatly benefited from advancements in semidefinite programming. The two-methods for solving SDPs discussed in Chapter 2 are some of the fastest known first-order methods. Further improvements to the computational implementation of these methods through parallelism and GPU coding can only expand their use. Investigation of other first-order algorithms, such as block-decomposition [11], may lead to methods that can efficiently compute solutions to significantly larger SDPs.

One route that is already being pursued is the inclusion of second order information to improve the number of iterations required to solve the SDP by the RRSDP method. Because SDPs for many chemical systems are not memory intensive including Hessian information is

a reasonable next step [7]. Second order information is included in non-linear programming by solving the first order KKT conditions with Newton's method to generate an update for the next iteration [10, 2, 5, 3]. The first order KKT conditions for the RRSDP method are

$$\nabla_x L_0(x,\lambda) = \nabla_x f(x) - \nabla_x h(x)[\lambda] = 0 \tag{7.1}$$

$$h(x) = 0 \tag{7.2}$$

where the $L_0()$ is the unaugmented Lagrangian and $h(x)$ is the linear constraints on the density matrix. If one considers a Newton solution to this system of equations

$$\begin{bmatrix} \nabla^2_{xx} L_0[x,\lambda] & -\nabla_x h(x) \\ -\nabla_x h(x)^T & 0 \end{bmatrix} \begin{bmatrix} \hat{x} - x \\ \hat{\lambda} - \lambda \end{bmatrix} = - \begin{bmatrix} \nabla_x L_0[x,\lambda] \\ h(x) \end{bmatrix} \tag{7.3}$$

we arrive at the second order update for the dual multipliers

$$\hat{\lambda} = \lambda + [B_k]^{-1}\,[h(x)] \tag{7.4}$$

$$B_k = \nabla_x h(x)^T [\nabla^2_{xx} L_0(x,\lambda)]^{-1} \nabla_x h(x). \tag{7.5}$$

Two alternative algorithms to the first-order update have been prosed by Ito and Kunisch [5]. Both involve solving the system of linear equations in Eq. 7.3 and using the new multipliers $\{\hat{\lambda}\}$ in the minimization of the augmented Lagrangian or taking the updated x as the next primal iterate. The Hessian takes on the form

$$\nabla^2_{xx} L_0(x,y) = \mathcal{I}_N \otimes \left(C - \sum_{y=i}^{m} y_i A_i \right) \tag{7.6}$$

where $\mathcal{I}_N$ is the identity matrix of rank N (N being the number of variables in primal solution). This Hessian recently appeared in Ref. [6] which formulates the RRSDP method

with the above second order update as a sequential quadratic program. This method is attractive because it removes the slow step of performing an unconstrained minimization on the augmented Lagrangian.

I believe that advancements in SDP methods either algorithmically or computationally can have a profound effect on what types of problems variational 2-RDM can solve. For systems with periodic boundaries this would facilitate extending the variational 2-RDM method to two- and three-dimensions. For molecular systems this would allow for the inclusion of significantly more orbitals in active spaces resulting in definitive answers to multireference type problems. Ultimately, variational 2-RDM holds great promise for describing electron correlation in quantum many body problems. Continued development will greatly benefit quantum chemistry and the solid-state communities.

7.4 References

[1] James S.M. Anderson, Maho Nakata, Ryo Igarashi, Katsuki Fujisawa, and Makoto Yamashita. The second-order reduced density matrix method and the two-dimensional hubbard model. *Computational and Theoretical Chemistry*, 1003:22 – 27, 2013. Reduced Density Matrices: A Simpler Approach to Many-Electron Problems?

[2] Dimitri P Bertsekas. Multiplier methods: a survey. *Automatica*, 12(2):133–145, 1976.

[3] Samuel Burer and Renato DC Monteiro. A nonlinear programming algorithm for solving semidefinite programs via low-rank factorization. *Mathematical Programming*, 95(2):329–357, 2003.

[4] C. A. Coulson. Present state of molecular structure calculations. *Rev. Mod. Phys.*, 32:170–177, Apr 1960.

[5] Kazufumi Ito and Karl Kunisch. Augmented lagrangian-sqp methods for nonlinear

optimal control problems of tracking type. *SIAM Journal on Control and Optimization*, 34(3):874–891, 1996.

[6] Kazuma IWASAKI. A hybrid algorithm of gradient and newton methods for semidefinite programs. Master's thesis, Kyoto University, 2015.

[7] David A. Mazziotti. First-order semidefinite programming for the direct determination of two-electron reduced density matrices with application to many-electron atoms and molecules. *The Journal of Chemical Physics*, 121(22), 2004.

[8] David A. Mazziotti. Significant conditions for the two-electron reduced density matrix from the constructive solution of n representability. *Phys. Rev. A*, 85:062507, Jun 2012.

[9] David A. Mazziotti. Structure of fermionic density matrices: Complete n-representability conditions. *Phys. Rev. Lett.*, 108:263002, Jun 2012.

[10] Angelo Miele and AV Levy. Modified quasilinearization and optimal initial choice of the multipliers part 1?mathematical programming problems. *Journal of Optimization Theory and Applications*, 6(5):364–380, 1970.

[11] Renato DC Monteiro, Camilo Ortiz, and Benar F Svaiter. Implementation of a block-decomposition algorithm for solving large-scale conic semidefinite programming problems. *Computational Optimization and Applications*, 57(1):45–69, 2014.

[12] Ward Poelmans, Mario Van Raemdonck, Brecht Verstichel, Stijn De Baerdemacker, Alicia Torre, Luis Lain, Gustavo E Massaccesi, Diego R Alcoba, Patrick Bultinck, and Dimitri Van Neck. Variational optimization of the second-order density matrix corresponding to a seniority-zero configuration interaction wave function. *Journal of chemical theory and computation*, 11(9):4064–4076, 2015.

[13] Brecht Verstichel, Ward Poelmans, Stijn De Baerdemacker, Sebastian Wouters, and Dimitri Van Neck. Variational optimization of the 2dm: approaching three-index accu-

racy using extended cluster constraints. *The European Physical Journal B*, 87(3):1–11, 2014.

[14] Brecht Verstichel, Helen van Aggelen, Ward Poelmans, Sebastian Wouters, and Dimitri Van Neck. Extensive v2dm study of the one-dimensional hubbard model for large lattice sizes: Exploiting translational invariance and parity. *Computational and Theoretical Chemistry*, 1003:12 – 21, 2013. Reduced Density Matrices: A Simpler Approach to Many-Electron Problems?